



Continuum shape sensitivity analysis of a mixed-mode fracture in functionally graded materials

B.N. Rao ^{a,*}, S. Rahman ^b

^a *Structural Engineering Division, Department of Civil Engineering, Indian Institute of Technology Madras, Chennai 600 036, India*

^b *Center for Computer-Aided Design, The University of Iowa, 220 Engineering Research Facility, Iowa City, IA 52242-1000, United States*

Received 10 September 2003; received in revised form 10 May 2004; accepted 15 June 2004

Abstract

This paper presents two new methods for conducting a continuum shape sensitivity analysis of a crack in an isotropic, linear-elastic functionally graded material. These methods involve the material derivative concept from continuum mechanics, domain integral representation of interaction integrals, known as the M -integral, and direct differentiation. Unlike virtual crack extension techniques, no mesh perturbation is needed to calculate the sensitivity of stress–intensity factors. Since the governing variational equation is differentiated prior to the process of discretization, the resulting sensitivity equations are independent of approximate numerical techniques, such as the meshless method, finite element method, boundary element method, or others. Three numerical examples are presented to calculate the first-order derivative of the stress–intensity factors. The results show that first-order sensitivities of stress intensity factors obtained using the proposed method are in excellent agreement with the reference solutions obtained using the finite-difference method for the structural and crack geometries considered in this study.

© 2004 Elsevier B.V. All rights reserved.

Keywords: Crack; Functionally graded materials; Interaction integral; M -integral; Linear-elastic fracture mechanics; Shape sensitivity analysis; Material derivative

* Corresponding author. Tel.: +91 44 22578498; fax: +91 44 22578327.

E-mail address: bnrao@iitm.ac.in (B.N. Rao).

URL: <http://www.civil.iitm.ac.in/people/faculty/nageswararao.html>

1. Introduction

Functionally graded materials (FGMs) that possess spatially varying microstructure and mechanical/thermal properties are essentially multi-phase particulate composites, engineered to meet a predetermined functional performance [1,2]. In recent years, various theoretical, computational, and experimental studies have been conducted to understand the fracture behavior of FGMs. A collection of technical papers, published in [3] reflects state-of-the-art research into FGM fracture. A major component of such studies involves calculating the crack-driving forces in FGMs both accurately and efficiently. Consequently, various numerical methods have been developed for calculating stress–intensity factors (SIFs), and can be found in the above-mentioned literature. More recently in 2003, Rao and Rahman [4,5] developed two interaction integrals for the mixed-mode fracture analysis of cracks in isotropic and orthotropic FGMs. In contrast to existing methods, it is not necessary to perform integration along the crack face of the discontinuity. Hence, the interaction integral method is simpler and more efficient than previously existing methods.

While past studies demonstrate a better understanding of FGM fracture, they also indicate areas of future development. For example, in many fracture mechanics applications, either the derivatives or sensitivities of SIF with respect to crack size are needed for predicting stability and arresting crack propagation in FGM. Another major use of SIF derivatives is in the reliability analysis of cracked structures. For example, the first- and second-order reliability methods [6], frequently used in probabilistic fracture mechanics [7–13], require the gradient and Hessian of the performance function with respect to crack length. In a linear-elastic fracture, the performance function builds on SIF. Hence, both first- and second-order derivatives of SIF are needed for probabilistic analysis of FGMs.

For predicting sensitivities of SIF under a mode-I condition, some methods have already appeared for homogenous materials. In 1988, Lin and Abel [14] employed a virtual crack extension technique [15–18] and the variational formulation in conjunction with the finite element method (FEM) to calculate the first-order derivative of SIF for a structure containing a single crack. Subsequently, Hwang et al. [19] generalized this method to calculate both first- and second-order derivatives for structures involving multiple crack systems, an axisymmetric stress state, and crack-face and thermal loading. However, these methods require mesh perturbation, a fundamental requirement of all virtual crack extension techniques. For second-order derivatives, the number of elements surrounding the crack tip affected by mesh perturbation has a significant effect on solution accuracy. To overcome this problem, Chen et al. [20–22] recently applied concepts from shape sensitivity analysis to calculate the first-order derivative of SIFs. In this new method, the domain integral representation of the J -integral (mode-I) or the interaction integral (mixed-mode) is invoked and the material derivative concept from continuum mechanics is then used to obtain the first-order sensitivity of SIFs. Since the governing variational equation is differentiated before discretization, the resulting sensitivity equations are independent of any approximate numerical techniques, such as FEM, the boundary element method, or others. However, most of the analytical methods discussed above are developed for the sensitivity analysis of cracks in homogenous materials. Only recently, Rao and Rahman [23] developed a sensitivity analysis method for a crack in an isotropic, linear-elastic FGM under mode-I loading conditions. Hence, there is a clear need to develop similar sensitivity equations for mixed-mode loading conditions.

This paper presents a new method for predicting the first-order sensitivity of mode-I and mode-II stress–intensity factors, K_I and K_{II} , respectively, for a crack in an isotropic, linear-elastic FGM. This method uses the material derivative concept from continuum mechanics, domain integral representation of an interaction integral, known as the M -integral, and direct differentiation. Unlike virtual crack extension techniques, no mesh perturbation is needed in the proposed method to calculate the sensitivity of stress–intensity factors. Since the governing variational equation is differentiated prior to the process of discretization, resulting sensitivity equations are independent of such approximate numerical techniques as the meshless method, the finite element method, the boundary element method, or others. Numerical examples are presented to calculate the first-order derivative of the M -integral and stress–intensity factors using the pro-

posed method. Numerical results of the first-order sensitivities of stress–intensity factors obtained using the proposed method are compared with reference solutions obtained from using finite-difference methods.

2. Shape sensitivity analysis

2.1. Velocity field

Consider a general three-dimensional body with a specific configuration, referred to as the reference configuration, with domain Ω , boundary Γ , and a body material point identified by position vector $\mathbf{x} \in \Omega$. Consider the motion of the body as it travels away from the reference configuration and into another configuration with domain Ω_τ and boundary Γ_τ , as shown in Fig. 1. This process can be expressed as

$$\mathbf{T} : \mathbf{x} \rightarrow \mathbf{x}_\tau, \quad \mathbf{x} \in \Omega, \tag{1}$$

where \mathbf{x} and \mathbf{x}_τ are the position vectors of a material point in the reference and perturbed configuration, respectively, \mathbf{T} is a transformation mapping, and τ is a scalar time like parameter denoting the amount of shape change, with

$$\begin{aligned} \mathbf{x}_\tau &= \mathbf{T}(\mathbf{x}, \tau), \\ \Omega_\tau &= \mathbf{T}(\Omega, \tau), \\ \Gamma_\tau &= \mathbf{T}(\Gamma, \tau). \end{aligned} \tag{2}$$

A velocity field \mathbf{V} can then be defined as

$$\mathbf{V}(\mathbf{x}_\tau, \tau) = \frac{d\mathbf{x}_\tau}{d\tau} = \frac{d\mathbf{T}(\mathbf{x}, \tau)}{d\tau} = \frac{\partial \mathbf{T}(\mathbf{x}, \tau)}{\partial \tau}. \tag{3}$$

In the neighborhood of an initial time $\tau = 0$, assuming a regularity hypothesis and ignoring high-order terms, \mathbf{T} can be approximated by

$$\mathbf{T}(\mathbf{x}, \tau) = \mathbf{T}(\mathbf{x}, 0) + \tau \frac{\partial \mathbf{T}(\mathbf{x}, 0)}{\partial \tau} + O(\tau^2) \cong \mathbf{x} + \tau \mathbf{V}(\mathbf{x}, 0), \tag{4}$$

where $\mathbf{x} = \mathbf{T}(\mathbf{x}, 0)$ and $\mathbf{V}(\mathbf{x}) = \mathbf{V}(\mathbf{x}, 0)$.

2.2. Sensitivity analysis

The variational governing equation for a non-homogeneous or homogeneous structural component with domain Ω can be formulated as [24,25]

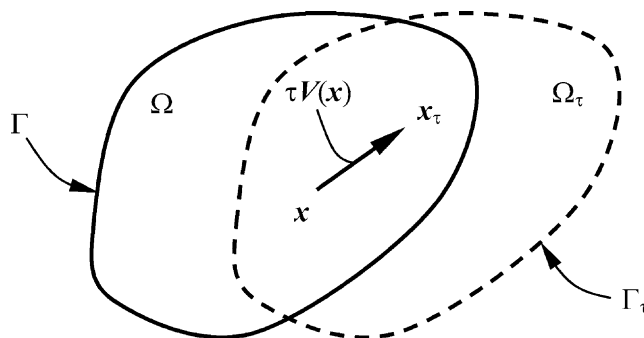


Fig. 1. Variation of domain.

$$a_{\Omega}(\mathbf{z}, \bar{\mathbf{z}}) = \ell_{\Omega}(\bar{\mathbf{z}}) \quad \text{for all } \bar{\mathbf{z}} \in \mathbf{Z}, \quad (5)$$

where \mathbf{z} and $\bar{\mathbf{z}}$ are the actual and virtual displacement fields of the structure, respectively, \mathbf{Z} is the space of kinematically admissible virtual displacements, and $a_{\Omega}(\mathbf{z}, \bar{\mathbf{z}})$ and $\ell_{\Omega}(\bar{\mathbf{z}})$ are energy quadratic and load linear forms, respectively. The subscript Ω in Eq. (5) is used to indicate the governing equation's dependence on the shape of the structural domain.

The pointwise material derivative at $\mathbf{x} \in \Omega$ is defined as [24,25]

$$\dot{\mathbf{z}} = \lim_{\tau \rightarrow 0} \left[\frac{\mathbf{z}_{\tau}(\mathbf{x} + \tau \mathbf{V}(\mathbf{x})) - \mathbf{z}(\mathbf{x})}{\tau} \right]. \quad (6)$$

If \mathbf{z}_{τ} has a regular extension into a neighborhood of Ω_{τ} , then

$$\dot{\mathbf{z}}(\mathbf{x}) = \mathbf{z}'(\mathbf{x}) + \nabla \mathbf{z}'^T \mathbf{V}(\mathbf{x}), \quad (7)$$

where

$$\mathbf{z}' = \lim_{\tau \rightarrow 0} \left[\frac{\mathbf{z}_{\tau}(\mathbf{x}) - \mathbf{z}(\mathbf{x})}{\tau} \right] \quad (8)$$

is the partial derivative of \mathbf{z} and $\nabla = \{\partial/\partial x_1, \partial/\partial x_2, \partial/\partial x_3\}^T$ is the vector of gradient operators. One attractive feature of the partial derivative is that, given the smoothness assumption, it commutes with the derivatives with respect to x_i , $i = 1, 2$, and 3 , since they are derivatives with respect to independent variables, i.e.,

$$\left(\frac{\partial \mathbf{z}}{\partial x_i} \right)' = \frac{\partial}{\partial x_i} (\mathbf{z}'), \quad i = 1, 2, \text{ and } 3. \quad (9)$$

Let ψ_1 be a domain functional, defined as an integral over Ω_{τ} , i.e.,

$$\psi_1 = \int_{\Omega_{\tau}} f_{\tau}(\mathbf{x}_{\tau}) d\Omega_{\tau}, \quad (10)$$

where f_{τ} is a regular function defined on Ω_{τ} . If Ω is C^k regular, then the material derivative of ψ_1 at Ω is [24,25]

$$\dot{\psi}_1 = \int_{\Omega} [f'(\mathbf{x}) + \text{div}(f(\mathbf{x})\mathbf{V}(\mathbf{x}))] d\Omega. \quad (11)$$

For a functional form of

$$\psi_2 = \int_{\Omega_{\tau}} g(\mathbf{z}_{\tau}, \nabla \mathbf{z}_{\tau}) d\Omega_{\tau}, \quad (12)$$

the material derivative of ψ_2 at Ω can be found using Eqs. (10) and (12), as [25]

$$\dot{\psi}_2 = \int_{\Omega_{\tau}} [g_{,z_i} \dot{z}_i - g_{,z_{ij}} (z_{i,j} V_j) + g_{,z_{ij}} \dot{z}_{i,j} - g_{,z_{ijk}} (z_{i,jk} V_k) + \text{div}(g\mathbf{V})] d\Omega, \quad (13)$$

in which a comma is used to denote partial differentiation, e.g., $z_{i,j} = \partial z_i / \partial x_j$, $z_{i,jk} = \partial^2 z_i / \partial x_j \partial x_k$, $\dot{z}_{i,j} = \partial \dot{z}_i / \partial x_j$, $g_{,z_i} = \partial g / \partial z_i$, $g_{,z_{ij}} = \partial g / \partial z_{ij}$ and V_j is the j th component of \mathbf{V} . In Eq. (13), the material derivative $\dot{\mathbf{z}}$ is the solution to the sensitivity equation obtained by taking the material derivative of Eq. (5).

If no body force is involved, the variational equation (Eq. (5)) can be written as

$$a_{\Omega}(\mathbf{z}, \bar{\mathbf{z}}) \equiv \int_{\Omega} \sigma_{ij}(\mathbf{z}) \varepsilon_{ij}(\bar{\mathbf{z}}) d\Omega = \ell_{\Omega}(\bar{\mathbf{z}}) \equiv \int_{\Gamma} T_i \bar{z}_i d\Gamma, \quad (14)$$

where $\sigma_{ij}(\mathbf{z})$ and $\varepsilon_{ij}(\bar{\mathbf{z}})$ are components of the stress and strain tensors of the displacement \mathbf{z} and virtual displacement $\bar{\mathbf{z}}$, respectively, T_i is the i th component of the surface traction, and \bar{z}_i is the i th component of $\bar{\mathbf{z}}$. Taking the material derivative of both sides of Eq. (14) and using Eq. (9),

$$a_\Omega(\dot{\mathbf{z}}, \bar{\mathbf{z}}) = \ell'_V(\bar{\mathbf{z}}) - a'_V(\mathbf{z}, \bar{\mathbf{z}}) \quad \forall \bar{\mathbf{z}} \in \mathbf{Z}, \tag{15}$$

where the subscript V indicates the dependency of the terms on the velocity field. The terms $\ell'_V(\bar{\mathbf{z}})$ and $a'_V(\mathbf{z}, \bar{\mathbf{z}})$ can be further derived as [24,25]

$$\ell'_V(\bar{\mathbf{z}}) = \int_\Gamma \{ -T_i(\bar{z}_{i,j}V_j) + [(T_i\bar{z}_i)_{,j}n_j + \kappa_\Gamma(T_i\bar{z}_i)](V_i n_i) \} d\Gamma \tag{16}$$

and

$$a'_V(\mathbf{z}, \bar{\mathbf{z}}) = \int_\Omega [\sigma_{ij}(\mathbf{z})(\bar{z}_{i,k}V_{k,j}) + \sigma_{ij}(\mathbf{z})(z_{i,k}V_{k,j}) - \varepsilon_{ij}(\bar{\mathbf{z}})D_{ijkl,m}\varepsilon_{kl}(\mathbf{z})V_m - \sigma_{ij}(\mathbf{z})\varepsilon_{ij}(\bar{\mathbf{z}})\text{div}V] d\Omega, \tag{17}$$

where n_i is the i th component of unit normal vector \mathbf{n} , κ_Γ is the curvature of the boundary, $z_{i,j} = \partial z_i / \partial x_j$, $\bar{z}_{i,j} = \partial \bar{z}_i / \partial x_j$, $V_{i,j} = \partial V_i / \partial x_j$, D_{ijkl} is the constitutive tensor, and $D_{ijkl,m} = \partial D_{ijkl} / \partial x_m$. Note that the third term in the integrand on the right hand side of Eq. (17) arises naturally in the formulation of a continuum shape sensitivity analysis for non-homogeneous materials, but vanishes for homogeneous materials. If the modulus of elasticity $E(\mathbf{x})$ is the only material property that varies, then $D_{ijkl,m} = (\partial E(\mathbf{x}) / \partial x_m) D_{ijkl} / E(\mathbf{x})$.

To evaluate the sensitivity expression of Eq. (13), a numerical method is needed to solve Eq. (14), for which a standard FEM was used. If the solution \mathbf{z} is obtained for Eq. (14) using an FEM code, the same code can be used to solve Eq. (15) for $\dot{\mathbf{z}}$. This solution can be obtained efficiently since it only requires an evaluation of the same set of FEM matrix equations with a different fictitious load, which is the right hand side of Eq. (15).

3. The interaction integral

Consider a linear-elastic, isotropic, two-dimensional cracked FGM with a rectilinear crack of length $2a$, subjected to external loads S_1, S_2, \dots, S_m , as shown in Fig. 2. It is assumed that the modulus of elasticity is the only material property that varies, according to

$$E = E(x_1, x_2) = E(\mathbf{x}), \tag{18}$$

where $\mathbf{x} = \{x_1, x_2\}^T \in \mathfrak{R}^2$, $E(\mathbf{x}) \geq 0$ is a continuous, bounded, and at least piecewise differentiable function on domain Ω , and x_1-x_2 is the coordinate system. In reality, FGMs are multi-phase materials with generally, locally discontinuous material properties. Hence, $E(x_1, x_2)$ in Eq. (18) should be viewed as the smoothly varying ‘‘effective’’ material properties of FGM. Poisson’s ratio ν was also held constant, which is a reasonable assumption, since variation in Poisson’s ratio is usually smaller than that of the elastic modulus.

Consider two independent equilibrium states of the cracked body. Let state 1 correspond to the *actual* state for the given boundary conditions, and let state 2 correspond to an *auxiliary* state, which comprises either mode-I or mode-II near tip displacement and stress fields. Superposition of these two states leads to another equilibrium state (say, state S), for which the domain form of the J -integral is

$$\begin{aligned} J^{(S)} = & \int_A \left((\sigma_{ij}^{(1)} + \sigma_{ij}^{(2)}) \frac{\partial(z_i^{(1)} + z_i^{(2)})}{\partial x_1} - (W^{(1)} + W^{(2)} + W^{(1,2)})\delta_{1j} \right) \frac{\partial q}{\partial x_j} dA \\ & + \int_A \left((\sigma_{ij}^{(1)} + \sigma_{ij}^{(2)}) \left(\frac{\partial^2 z_i^{(2)}}{\partial x_j \partial x_1} - \frac{\partial \varepsilon_{ij}^{(2)}}{\partial x_1} \right) - \frac{1}{2} (\varepsilon_{ij}^{(1)} + \varepsilon_{ij}^{(2)}) \frac{\partial D_{ijkl}}{\partial x_1} (\varepsilon_{kl}^{(1)} + \varepsilon_{kl}^{(2)}) \right) q dA, \end{aligned} \tag{19}$$

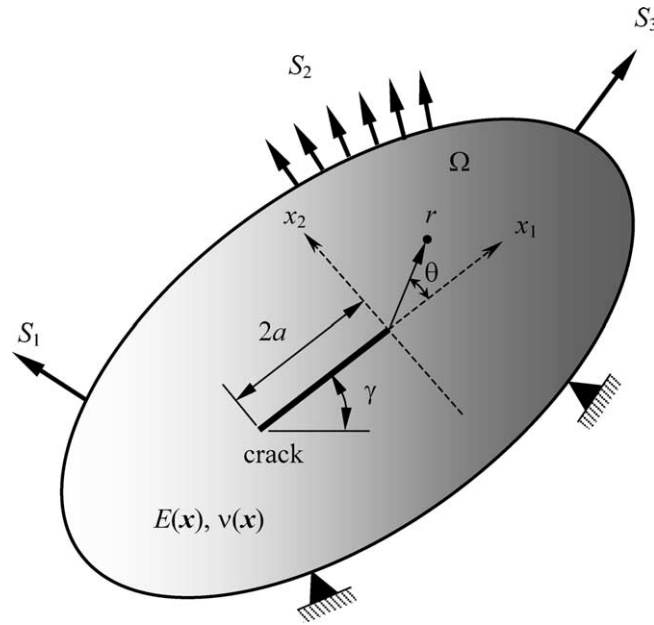


Fig. 2. General cracked body under mixed-mode loading.

where $W = \int \sigma_{ij} d\epsilon_{ij}$ is the strain energy density, $W^{(1,2)} = \frac{1}{2}(\sigma_{ij}^{(1)} \epsilon_{ij}^{(2)} + \sigma_{ij}^{(2)} \epsilon_{ij}^{(1)})$ is the mutual strain energy from the two states, δ_{ij} is the Kronecker delta, A is the area inside the contour, q is a weight function, and the superscripts denote various equilibrium states. In comparing Eq. (19) to the classical J -integral, the presence of material non-homogeneity results in the addition of the second domain integral. The J -integral, which also represents the energy release rate of an elastic body, becomes zero for any closed contour in an uncracked homogeneous (as well as non-homogeneous) body, and therefore, remains path-independent when used in conjunction with cracks in FGM. By expanding Eq. (19), it can be shown that [4]

$$J^{(S)} = J^{(1)} + J^{(2)} + M^{(1,2)}, \quad (20)$$

where $J^{(1)}$ and $J^{(2)}$ are the J -integrals for states 1 and 2, respectively, and $M^{(1,2)}$ is an interaction integral. Clearly, evaluations of $J^{(S)}$ and the resulting interaction integral are dependent on how the auxiliary field is defined, and several options are available. Two methods proposed by Rao and Rahman [4] are summarized as follows.

3.1. Method I—Homogeneous auxiliary field

Method I involves selecting auxiliary stress and displacement fields given by either mode-I or mode-II near tip displacement and stress fields. The auxiliary strain field is calculated from the symmetric gradient of the auxiliary displacement field. In this approach, the auxiliary stress and strain fields are related through a constant constitutive tensor evaluated at the crack tip. Hence, both the equilibrium condition ($\partial \sigma_{ij}^{(2)} / \partial x_j = 0$) and the strain–displacement relation ($\epsilon_{ij}^{(2)} = \partial z_i^{(2)} / \partial x_j$) are satisfied in the auxiliary state. However, the non-homogeneous constitutive relation of FGM is not strictly satisfied in the auxiliary state, yielding [4]

$$\begin{aligned}
 M^{(1,2)} &= \int_A \left[\sigma_{ij}^{(1)} \frac{\partial z_i^{(2)}}{\partial x_1} + \sigma_{ij}^{(2)} \frac{\partial z_i^{(1)}}{\partial x_1} - W^{(1,2)} \delta_{1j} \right] \frac{\partial q}{\partial x_j} dA \\
 &+ \int_A \frac{1}{2} \left[\sigma_{ij}^{(1)} \frac{\partial \varepsilon_{ij}^{(2)}}{\partial x_1} - \frac{\partial \sigma_{ij}^{(2)}}{\partial x_1} \varepsilon_{ij}^{(1)} + \sigma_{ij}^{(2)} \frac{\partial \varepsilon_{ij}^{(1)}}{\partial x_1} - \frac{\partial \sigma_{ij}^{(1)}}{\partial x_1} \varepsilon_{ij}^{(2)} \right] q dA.
 \end{aligned} \tag{21}$$

3.2. Method II—Non-homogeneous auxiliary field

Method II entails selecting the auxiliary stress and displacement fields given by either mode-I or mode-II near tip displacement and stress fields. The auxiliary strain field is calculated from the auxiliary stress field using the same spatially varying constitutive tensor from FGM. In this approach, the auxiliary stress field satisfies the equilibrium condition ($\partial \sigma_{ij}^{(2)} / \partial x_j = 0$); however, the auxiliary strain field is not compatible with the auxiliary displacement field ($\varepsilon_{ij}^{(2)} \neq \partial z_i^{(2)} / \partial x_j$). Since the auxiliary fields are not compatible, this method also introduces additional terms to the resulting interaction integral, i.e. [4],

$$\begin{aligned}
 M^{(1,2)} &= \int_A \left[\sigma_{ij}^{(1)} \frac{\partial z_i^{(2)}}{\partial x_1} + \sigma_{ij}^{(2)} \frac{\partial z_i^{(1)}}{\partial x_1} - W^{(1,2)} \delta_{1j} \right] \frac{\partial q}{\partial x_j} dA \\
 &+ \int_A \left[\sigma_{ij}^{(1)} \left(\frac{\partial^2 z_i^{(2)}}{\partial x_j \partial x_1} - \frac{\partial \varepsilon_{ij}^{(2)}}{\partial x_1} \right) - \varepsilon_{ij}^{(1)} \frac{\partial D_{ijkl}}{\partial x_1} \varepsilon_{kl}^{(2)} \right] q dA.
 \end{aligned} \tag{22}$$

Since the auxiliary strain field is calculated from the auxiliary stress field using the same spatially varying constitutive tensor of FGM, Eq. (22) can be rewritten as

$$\begin{aligned}
 M^{(1,2)} &= \int_A \left[\sigma_{ij}^{(1)} \frac{\partial z_i^{(2)}}{\partial x_1} + \sigma_{ij}^{(2)} \frac{\partial z_i^{(1)}}{\partial x_1} - W^{(1,2)} \delta_{1j} \right] \frac{\partial q}{\partial x_j} dA \\
 &+ \int_A \left[\sigma_{ij}^{(1)} \left(\frac{\partial \varepsilon_{ij}^{(2)}}{\partial x_1} - \frac{\partial \tilde{\varepsilon}_{ij}^{(2)}}{\partial x_1} \right) - \varepsilon_{ij}^{(1)} \frac{\partial D_{ijkl}}{\partial x_1} \varepsilon_{kl}^{(2)} \right] q dA,
 \end{aligned} \tag{23}$$

where $\tilde{\varepsilon}_{ij}^{(2)} = C_{ijkl} \sigma_{ij}^{(2)}$ with C_{ijkl} representing the compliance tensor. In Eq. (19) and (21)–(23), the auxiliary state for stresses and displacements is

$$\left\{ \begin{matrix} \sigma_{11}^{(2)} \\ \sigma_{22}^{(2)} \\ \sigma_{12}^{(2)} \end{matrix} \right\} = \frac{1}{\sqrt{2\pi r}} \left\{ \begin{matrix} \cos \frac{\theta}{2} \left(1 - \sin \frac{\theta}{2} \sin \frac{3\theta}{2} \right) \\ \cos \frac{\theta}{2} \left(1 + \sin \frac{\theta}{2} \sin \frac{3\theta}{2} \right) \\ \cos \frac{\theta}{2} \sin \frac{\theta}{2} \cos \frac{3\theta}{2} \end{matrix} \right\} \tag{24}$$

and

$$\left\{ \begin{matrix} z_1^{(2)} \\ z_2^{(2)} \end{matrix} \right\} = \frac{1}{2\mu_{tip}} \sqrt{\frac{r}{2\pi}} \left\{ \begin{matrix} \cos \frac{\theta}{2} \left[\kappa - 1 + 2\sin^2 \frac{\theta}{2} \right] \\ \sin \frac{\theta}{2} \left[\kappa + 1 - 2\cos^2 \frac{\theta}{2} \right] \end{matrix} \right\} \tag{25}$$

and

$$\begin{Bmatrix} \sigma_{11}^{(2)} \\ \sigma_{22}^{(2)} \\ \sigma_{12}^{(2)} \end{Bmatrix} = \frac{1}{\sqrt{2\pi r}} \begin{Bmatrix} -\sin \frac{\theta}{2} \left[2 + \cos \frac{\theta}{2} \cos \frac{3\theta}{2} \right] \\ \sin \frac{\theta}{2} \cos \frac{\theta}{2} \cos \frac{3\theta}{2} \\ \cos \frac{\theta}{2} \left[1 - \sin \frac{\theta}{2} \sin \frac{3\theta}{2} \right] \end{Bmatrix} \quad (26)$$

and

$$\begin{Bmatrix} z_1^{(2)} \\ z_2^{(2)} \end{Bmatrix} = \frac{1}{2\mu_{\text{tip}}} \sqrt{\frac{r}{2\pi}} \begin{Bmatrix} \sin \frac{\theta}{2} \left[\kappa + 1 + 2\cos^2 \frac{\theta}{2} \right] \\ -\cos \frac{\theta}{2} \left[\kappa - 1 - 2\sin^2 \frac{\theta}{2} \right] \end{Bmatrix} \quad (27)$$

for mode-I and mode-II, respectively, where $\mu_{\text{tip}} = E_{\text{tip}}/[2(1 + \nu)]$ is the shear modulus, E_{tip} is the elastic modulus at the crack tip, and $\kappa = (3 - \nu)/(1 + \nu)$ for plane stress, and $\kappa = 3 - 4\nu$ for plane strain. Note that all quantities are evaluated with respect to a coordinate system with the crack tip as the origin. Also, the summation convention is adopted for repeated indices.

The energy release-rate interpretation of the J -integral in Eqs. (19) and (20) yields

$$M^{(1,2)} = \frac{2}{E_{\text{tip}}^*} \left[(K_{\text{I}}^{(1)} K_{\text{I}}^{(2)} + K_{\text{II}}^{(1)} K_{\text{II}}^{(2)}) \right], \quad (28)$$

where E_{tip}^* is given by E_{tip} under the plane stress condition and by $E_{\text{tip}}/[1 - \nu^2]$ under the plane strain condition, respectively. The individual SIFs for the *actual* state can be obtained by judiciously choosing the *auxiliary* state (state 2). For example, if state 2 is chosen to be state I (state II), i.e., the mode-I (mode-II) near tip displacement and stress field is chosen as the *auxiliary* state, then $K_{\text{I}}^{(2)} = 1(0)$ and $K_{\text{II}}^{(2)} = 0(1)$. In that case, Eq. (28) yields

$$K_{\text{I}}^{(1)} = \frac{M^{(1,\text{I})} E_{\text{tip}}^*}{2}, \quad (29)$$

$$K_{\text{II}}^{(1)} = \frac{M^{(1,\text{II})} E_{\text{tip}}^*}{2}. \quad (30)$$

In Eqs. (29) and (30), $M^{(1,\text{I})}$ and $M^{(1,\text{II})}$ are the two interaction integrals for modes I and II, respectively, and can easily be evaluated using Eq. (21) or (23). In contrast to existing methods [28], there is no need to perform integration along the crack face of the discontinuity. Hence, the proposed method is simpler and more efficient than existing methods. See Ref. [4] for further details. In this study, both Eqs. (21) and (23) were employed for sensitivity analysis, as described in the following section.

4. Sensitivity of interaction integral and stress–intensity factors

4.1. Method I—Homogeneous auxiliary field

The expansion of each term on the right side of Eq. (21) yields

$$M^{(1,2)} = \int_A p \, dA, \quad (31)$$

where

$$p = \sum_{i=1}^{26} p_i. \tag{32}$$

The explicit expressions of $p_i, i = 1, \dots, 26$ are given in Appendix A. In relation to Eq. (11), the material derivative of $M^{(1,2)}$ is

$$\dot{M}^{(1,2)} = \int_A [p' + \text{div}(pV)] dA, \tag{33}$$

where

$$p' = \sum_{i=1}^{26} p'_i, \tag{34}$$

$$V = \left\{ \begin{matrix} V_1(\mathbf{x}) \\ V_2(\mathbf{x}) \end{matrix} \right\} \tag{35}$$

is the velocity field, and

$$\text{div}(pV) = \frac{\partial(pV_1)}{\partial x_1} + \frac{\partial(pV_2)}{\partial x_2} = \sum_{i=1}^{26} \frac{\partial(p_i V_1)}{\partial x_1} + \sum_{i=1}^{26} \frac{\partial(p_i V_2)}{\partial x_2}. \tag{36}$$

Finally, Eq. (33) becomes

$$\dot{M}^{(1,2)} = \sum_{i=1}^{26} \int_A P_i dA, \tag{37}$$

where

$$P_i = p'_i + \frac{\partial(p_i V_1)}{\partial x_1} + \frac{\partial(p_i V_2)}{\partial x_2}, \quad i = 1, \dots, 26. \tag{38}$$

For illustrative purposes, consider the first term

$$P_1 = p'_1 + \frac{\partial(p_1 V_1)}{\partial x_1} + \frac{\partial(p_1 V_2)}{\partial x_2}, \tag{39}$$

which can be expanded to

$$\begin{aligned} P_1 &= \left(\sigma_{11}^{(1)} \frac{\partial z_1^{(2)}}{\partial x_1} \frac{\partial q}{\partial x_1} \right)' + \frac{\partial}{\partial x_1} \left(\sigma_{11}^{(1)} \frac{\partial z_1^{(2)}}{\partial x_1} \frac{\partial q}{\partial x_1} V_1 \right) + \frac{\partial}{\partial x_2} \left(\sigma_{11}^{(1)} \frac{\partial z_1^{(2)}}{\partial x_1} \frac{\partial q}{\partial x_1} V_2 \right) \\ &= \sigma_{11}^{(1)} \frac{\partial z_1^{(2)}}{\partial x_1} \frac{\partial q}{\partial x_1} + \sigma_{11}^{(1)} \frac{\partial z_1^{(2)}}{\partial x_1} \frac{\partial q}{\partial x_1} + \sigma_{11}^{(1)} \frac{\partial z_1^{(2)}}{\partial x_1} \frac{\partial q'}{\partial x_1} + \frac{\partial \sigma_{11}^{(1)}}{\partial x_1} \frac{\partial z_1^{(2)}}{\partial x_1} V_1 \frac{\partial q}{\partial x_1} + \sigma_{11}^{(1)} \frac{\partial^2 z_1^{(2)}}{\partial x_1^2} V_1 \frac{\partial q}{\partial x_1} \\ &\quad + \sigma_{11}^{(1)} \frac{\partial z_1^{(2)}}{\partial x_1} \frac{\partial V_1}{\partial x_1} \frac{\partial q}{\partial x_1} + \sigma_{11}^{(1)} V_1 \frac{\partial z_1^{(2)}}{\partial x_1} \frac{\partial^2 q}{\partial x_1^2} + \frac{\partial \sigma_{11}^{(1)}}{\partial x_2} \frac{\partial z_1^{(2)}}{\partial x_1} V_2 \frac{\partial q}{\partial x_1} + \sigma_{11}^{(1)} \frac{\partial^2 z_1^{(2)}}{\partial x_1 \partial x_2} V_2 \frac{\partial q}{\partial x_1} \\ &\quad + \sigma_{11}^{(1)} \frac{\partial z_1^{(2)}}{\partial x_1} \frac{\partial V_2}{\partial x_2} \frac{\partial q}{\partial x_1} + \sigma_{11}^{(1)} V_2 \frac{\partial z_1^{(2)}}{\partial x_1} \frac{\partial^2 q}{\partial x_1 \partial x_2}. \end{aligned} \tag{40}$$

In this study, the velocity field V was chosen in such a way that the finite element mesh in the domain over which the M -integral in the Eq. (21) or (23) is evaluated, has a virtual rigid body translation along with the crack tip. The velocity field V is constant in the region over which the M -integral is evaluated, varies

smoothly in rest of the domain, and is zero along the boundary. The velocity field will be explained in more detail in a forthcoming section. Since q is defined around the crack tip in the domain over which the M -integral is evaluated, if the crack tip moves, the value of q will be same around the new crack tip. Hence, $\dot{q} = 0$. Therefore,

$$q' = \dot{q} - \nabla V^T q V = -\nabla^T q V = -\frac{\partial q}{\partial x_1} V_1 - \frac{\partial q}{\partial x_2} V_2. \quad (41)$$

In addition, since the velocity field V is constant in the region over which the M -integral is evaluated,

$$\frac{\partial V_i}{\partial x_j} = 0, \quad i, j = 1, 2 \quad (42)$$

and

$$\frac{\partial^2 V_i}{\partial x_j \partial x_k} = 0, \quad i, j, k = 1, 2. \quad (43)$$

Eqs. (41) and (42) yield

$$\frac{\partial q'}{\partial x_1} = -\frac{\partial^2 q}{\partial x_1^2} V_1 - \frac{\partial^2 q}{\partial x_1 \partial x_2} V_2, \quad (44)$$

$$\frac{\partial q'}{\partial x_2} = -\frac{\partial^2 q}{\partial x_1 \partial x_2} V_1 - \frac{\partial^2 q}{\partial x_2^2} V_2. \quad (45)$$

Since $E(x)$ is independent of the change in crack length, $E' = 0$. Therefore,

$$\dot{E} = \nabla^T E V = \frac{\partial E}{\partial x_1} V_1 + \frac{\partial E}{\partial x_2} V_2. \quad (46)$$

Using Eqs. (7), (42), and the strain–displacement relationship, it can be shown that,

$$\varepsilon'_{11} = \frac{\partial \dot{z}_1^{(1)}}{\partial x_1} - \frac{\partial^2 z_1^{(1)}}{\partial x_1^2} V_1 - \frac{\partial^2 z_1^{(1)}}{\partial x_1 \partial x_2} V_2, \quad (47)$$

$$\varepsilon'_{22} = \frac{\partial \dot{z}_2^{(1)}}{\partial x_2} - \frac{\partial^2 z_2^{(1)}}{\partial x_2 \partial x_1} V_1 - \frac{\partial^2 z_2^{(1)}}{\partial x_2^2} V_2 \quad (48)$$

and

$$\varepsilon'_{12} = \frac{1}{2} \left(\frac{\partial \dot{z}_1^{(1)}}{\partial x_2} - \frac{\partial^2 z_1^{(1)}}{\partial x_2 \partial x_1} V_1 - \frac{\partial^2 z_1^{(1)}}{\partial x_2^2} V_2 + \frac{\partial \dot{z}_2^{(1)}}{\partial x_1} - \frac{\partial^2 z_2^{(1)}}{\partial x_1^2} V_1 - \frac{\partial^2 z_2^{(1)}}{\partial x_1 \partial x_2} V_2 \right). \quad (49)$$

From the stress–strain relationship, it follows that

$$\sigma'_{ij} = D_{ijkl} \varepsilon'_{kl}. \quad (50)$$

Substituting Eqs. (42), (44), (47) and (50) into Eq. (40), following by simplification, leads to

$$P_1 = \dot{\sigma}'_{11} \frac{\partial z_1^{(2)}}{\partial x_1} \frac{\partial q}{\partial x_1} + \sigma'_{11} \frac{\partial z_1^{(2)}}{\partial x_1} \frac{\partial q}{\partial x_1}, \quad (51)$$

where $\dot{\sigma}'_{11}$ is the material derivative of σ'_{11} , which is more explicitly defined in Eq. (A.41) of Appendix A. A similar procedure can be applied using Eqs. (41)–(50) to determine the remaining P -functions. The explicit expressions of P_i , $i = 1, \dots, 26$ are given in Appendix A.

4.2. Method II—Non-homogeneous auxiliary field

Similarly, the expansion of each term on the right side of Eq. (23) yields and noting that in obtaining Eq. (23), the auxiliary strain field is calculated from the auxiliary stress field using the same spatially varying constitutive tensor of FGM yields

$$M^{(1,2)} = \int_A s \, dA, \tag{52}$$

where

$$s = \sum_{i=1}^{14} s_i. \tag{53}$$

The explicit expressions of $s_i, i = 1, \dots, 14$ are given in Appendix B. In relation to Eq. (11), the material derivative of $M^{(1,2)}$ is

$$\dot{M}^{(1,2)} = \int_A [s' + \text{div} (sV)] \, dA, \tag{54}$$

where

$$s' = \sum_{i=1}^{14} s'_i \tag{55}$$

and

$$\text{div} (sV) = \frac{\partial(sV_1)}{\partial x_1} + \frac{\partial(sV_2)}{\partial x_2} = \sum_{i=1}^{14} \frac{\partial(s_i V_1)}{\partial x_1} + \sum_{i=1}^{14} \frac{\partial(s_i V_2)}{\partial x_2}. \tag{56}$$

Finally, Eq. (54) becomes

$$\dot{M}^{(1,2)} = \sum_{i=1}^{14} \int_A S_i \, dA, \tag{57}$$

where

$$S_i = s'_i + \frac{\partial(s_i V_1)}{\partial x_1} + \frac{\partial(s_i V_2)}{\partial x_2}, \quad i = 1, \dots, 14. \tag{58}$$

The explicit expressions of $S_i, i = 1, \dots, 14$ are given in Appendix B.

Eqs. (A.2)–(A.27) in Appendix A provide explicit expressions of $P_i, i = 1, \dots, 26$, and Eqs. (B.2)–(B.15) in Appendix B provide explicit expressions of $S_i, i = 1, \dots, 14$, which can be inserted into Eqs. (37) and (57), respectively, to yield the first-order sensitivity of $M^{(1,2)}$ with respect to crack size. The integral in Eqs. (37) and (57) are independent of the domain size A and can be calculated numerically using standard Gaussian quadrature. A 2×2 or higher integration rule is recommended for calculating \dot{M} . A flow diagram for calculating the sensitivity of M is shown in Fig. 3.

4.3. Sensitivities of stress–intensity factors

From Eqs. (29) and (30), the sensitivities of K_I and K_{II} can be calculated by

$$\frac{\partial K_I}{\partial a} = \frac{M^{(1,1)} E_{\text{tip}}^* + M^{(1,1)} \dot{E}_{\text{tip}}^*}{2\sqrt{V_{1,\text{tip}}^2 + V_{2,\text{tip}}^2}} \tag{59}$$

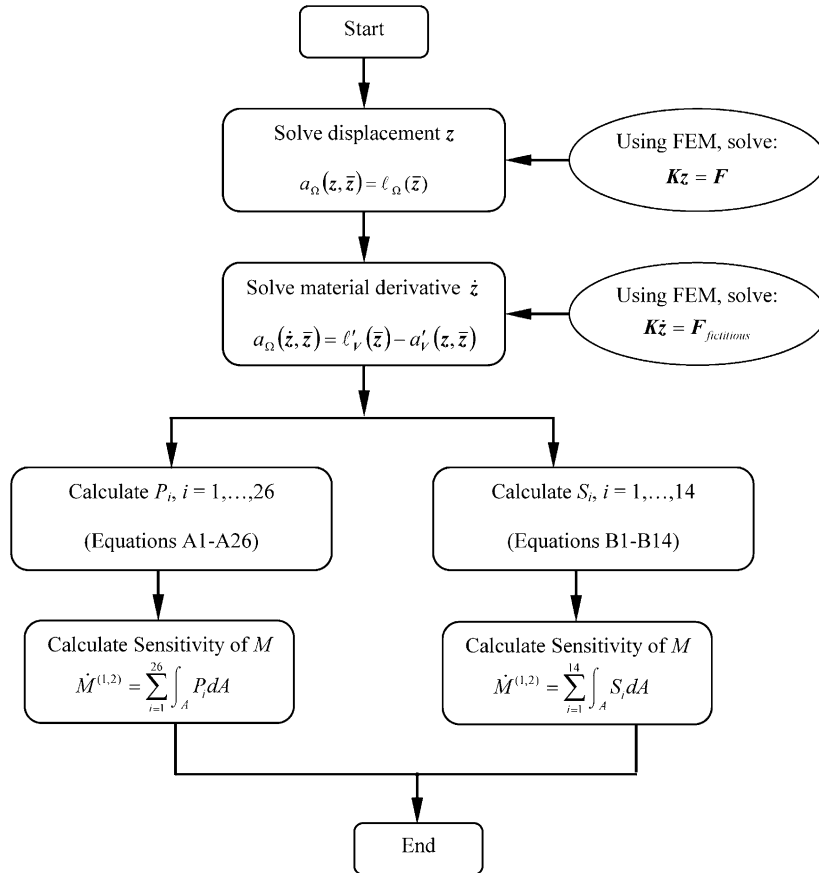


Fig. 3. A flowchart for continuum sensitivity analysis of crack size.

and

$$\frac{\partial K_{II}}{\partial a} = \frac{M^{(1,II)} E_{tip}^* + M^{(1,II)} \dot{E}_{tip}^*}{2\sqrt{V_{1,tip}^2 + V_{2,tip}^2}}, \tag{60}$$

respectively, where $V_{1,tip}$ and $V_{2,tip}$ are corresponding crack-tip velocities in x_1 - and x_2 directions, respectively, and \dot{E}_{tip}^* is equal to \dot{E}_{tip} under plane stress and $\dot{E}_{tip}/(1 - \nu^2)$ under plane strain, and \dot{E}_{tip} is equal to \dot{E} when evaluated at the crack-tip. According to Eqs. (59) and (60), the first-order sensitivities of K_I and K_{II} require material derivatives of interaction integral, which in turn can be evaluated using Eqs. (37) and (57). In this study, methods of sensitivity analysis involving Eqs. (37) and (57) are described as Method-I and Method-II, respectively.

4.4. Velocity field definition

The definition of the velocity field is an important step in continuum shape sensitivity analysis. Applying an inappropriate velocity field for shape sensitivity analysis will yield inaccurate sensitivity results. The velocity field must meet numerous, stringent theoretical and practical criteria [26–28]. Theoretically, (1)

the design velocity field must have the same regularity as the displacement field, and (2) depend linearly on the variation of shape design parameters. For two- and three-dimensional elastic solid problems C^0 design velocity fields with integrable first derivatives are required. The regularity requirement comes from the mathematical regularity of design velocity in the design sensitivity expression in Eq. (17). This requirement can also be met by using the displacement shape functions of the finite element analysis to represent design velocity fields. For practical applications, (1) the design velocity computation method must retain the topology of the original finite element mesh, (2) provide finite element boundary nodes that stay on the geometric boundary for all shape changes, (3) use a mathematical rule that guarantees linear dependency of finite element node movements on the variations of shape design parameters, (4) produce a finite element mesh that is not distorted, (5) be naturally linked to design parameters defined on a computer simulation model, (6) allow the mathematical rule to be reusable, and (7) be efficient and general for a large class of applications. A number of methods have been proposed in the literature to compute the velocity field [27,28]. Two types of velocity fields were adopted in this study using the proposed methods (Method-I and Method-II). For convenience, they are referred to as Velocity Field I and Velocity Field II. Both velocity fields satisfy the theoretical and practical criteria outlined above and ensure that the finite element mesh in the domain over which the SIFs and their sensitivities are evaluated has a virtual rigid body translation along with the crack tip. The following example illustrates the velocity fields that were adopted in this study.

Consider an edge-cracked plate with length L , width W and crack length a , as shown in Fig. 4(a). Also shown in Fig. 4(a), is a domain of size $2b \times 2b$, which was used to calculate the mixed-mode SIFs and their sensitivities. Then, the two velocity fields V adopted in this study can be defined.

Velocity Field I: Referring to Fig. 4(b), the C^0 continuous velocity field V with integrable first derivatives is defined as

$$V(\mathbf{x}) = \left\{ \begin{array}{l} V_1(\bar{x}_1, \bar{x}_2) \\ V_2(\bar{x}_1, \bar{x}_2) \end{array} \right\}, \quad (61)$$

where \bar{x}_1 – \bar{x}_2 axes are measured with respect to crack tip T_0 and are oriented in the direction of the x_1 – x_2 axes. More explicit forms of $V(\mathbf{x})$ that depend on crack geometry and which satisfy both the theoretical and practical criteria outlined above are defined in the subsequent section of numeric examples.

Velocity Field II: Velocity field V can be obtained by performing an FEM analysis. The same FEM discretization used in regular fracture analysis is adopted. The FEM analysis is performed by prescribing a velocity at the crack-tip ($V_{1,\text{tip}}$, $V_{2,\text{tip}}$), and at all nodes in the domain $2b \times 2b$, as shown in Fig. 4(b). A zero velocity field is prescribed on the boundary. The displacement response from FEM analysis and applied boundary conditions constitute the velocity field $V(\mathbf{x})$.

Both velocity fields were employed in the following numerical examples.

5. Numerical examples

Three numerical examples based on mixed-mode deformations are presented to illustrate Method-I and Method-II that have been proposed. In all examples, Poisson's ratio was held constant with $\nu = 0.3$, and a 2×2 Gaussian integration was employed. A perturbation of 10^{-5} times the crack length was used in finite-difference calculations to provide benchmark results. In the first example, both velocity fields were studied. The second and third examples employ Velocity Field I and Velocity Field II, respectively.

5.1. Example 1: Edge-cracked plate

This example involves the edge-cracked plate shown in Fig. 4(a), which is fixed at the bottom and subjected to far-field shear stress of $\tau^\infty = 1$ unit applied on top. The plate has length $L = 16$ units, width $W = 7$

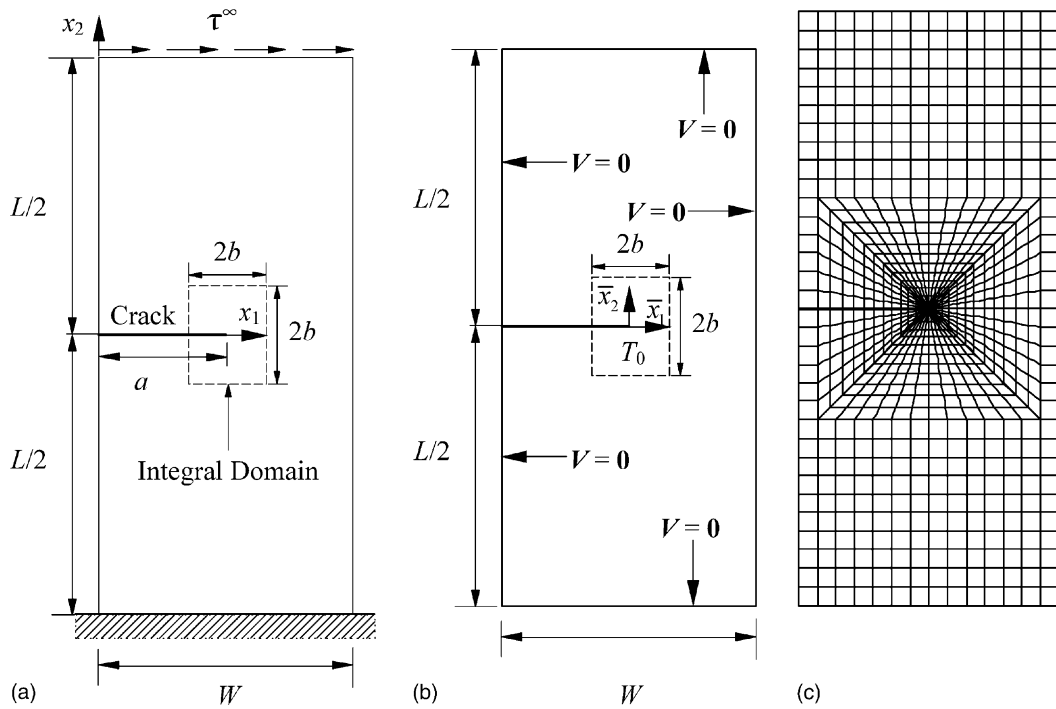


Fig. 4. Edge-cracked plate; (a) geometry, loads, and domain size; (b) velocity field definition; and (c) FEM discretization (2711 nodes, 832 8-noded quadrilateral elements and 48 focused quarter–point 6-noded triangular elements).

units and crack length $a = 3.5$ units. The elastic modulus was assumed to follow an exponential function, given by

$$E(x_1) = E_1 \exp\left(\frac{\eta x_1}{W}\right), \quad 0 \leq x_1 \leq W, \tag{62}$$

where $\eta = \ln(E_2/E_1)$ is the material parameter, $E_1 = E(0)$, and $E_2 = E(W)$. For numerical values, $E_1 = 1$ unit, and $E_2/E_1 = \exp(\eta) = 0.1, 0.2, 1, 5,$ and 10 were used. A plane strain condition was assumed. Both Methods I and II were used to calculate the mixed-mode SIFs and their sensitivities with a domain size $2b \times 2b$ ($b = 3.0$ units), as shown in Fig. 4(a). FEM discretization involved 2711 nodes, 832 8-noded quadrilateral elements, and 48 focused quarter-point 6-noded triangular elements, as shown in Fig. 4(c). Both types of velocity fields (Velocity Field I and Velocity Field II) were employed.

Velocity Field I is defined as

$$\begin{Bmatrix} V_1(\bar{x}_1, \bar{x}_2) \\ V_2(\bar{x}_1, \bar{x}_2) \end{Bmatrix} = V_{1,\text{tip}} \begin{Bmatrix} C_1(\bar{x}_1)C_2(\bar{x}_2) \\ 0 \end{Bmatrix}, \tag{63}$$

where

$$C_1(\bar{x}_1) = \begin{cases} 1 & \text{if } |\bar{x}_1| \leq 3.0, \\ \frac{x_1 - 3.5}{-0.5} & \text{if } \bar{x}_1 > 3.0, \\ \frac{x_1 + 3.5}{0.5} & \text{if } \bar{x}_1 < -3.0 \end{cases} \tag{64}$$

and

$$C_2(\bar{x}_2) = \begin{cases} 1 & \text{if } |\bar{x}_2| \leq 3.0, \\ \frac{4.0 - (|\bar{x}_2| - 3.0)}{7.0} & \text{if } |\bar{x}_2| > 3.0 \text{ and } |\bar{x}_2| \leq 7.0, \\ 0 & \text{if } |\bar{x}_2| > 7.0. \end{cases} \quad (65)$$

The \bar{x}_1 – \bar{x}_2 axes are measured with respect to the crack tip T_0 and are oriented in the direction of the x_1 – x_2 axes, as shown in Fig. 4(b). Velocity Field II involves FEM analysis, as described in a previous section. In both cases, the velocity field at the crack-tip, $(V_{1,\text{tip}}, V_{2,\text{tip}}) = (10^{-5}a, 0)$, was used for sensitivity analysis. Fig. 5 shows the contour plot of the variation of the V_1 component of Velocity Field I, whereas Fig. 6(a) and (b) schematically illustrates the variation of the V_1 and V_2 components of Velocity Field II over the entire domain of the edge-cracked plate.

Tables 1 and 2 show the predicted mixed-mode SIFs and their sensitivities for the edge-cracked problem, obtained in the present study for various values of E_2/E_1 using Method-I and Method-II for the two kinds of velocity fields. Two sets of results are shown for $\partial K_I/\partial a$ and $\partial K_{II}/\partial a$. The first set of results are computed using the proposed methods (Method-I and Method-II) and the second set are calculated using the finite-difference method. The results in Tables 1 and 2 demonstrate that continuum shape sensitivity analysis provides accurate estimates of $\partial K_I/\partial a$ and $\partial K_{II}/\partial a$ when compared with corresponding results from the finite-difference method for various values of E_2/E_1 , and irrespective of the kind of velocity fields. Using the proposed methods (Method-I and Method-II), the domain independence of mixed-mode SIFs and their sensitivities was verified by varying the sizes of the integral domain parameter. Tables 3–5 show the results of mixed-mode SIFs and their sensitivities for various values of E_2/E_1 using Method-I and Method-II for the integral domain parameter $b = 2.33, 1.74, \text{ and } 1.22$ units, respectively. The results in Tables 3–5 were obtained using Velocity Field I. Very accurate and stable results of mixed-mode SIFs and their sensitivities were obtained regardless of the integral domain size and type of method.

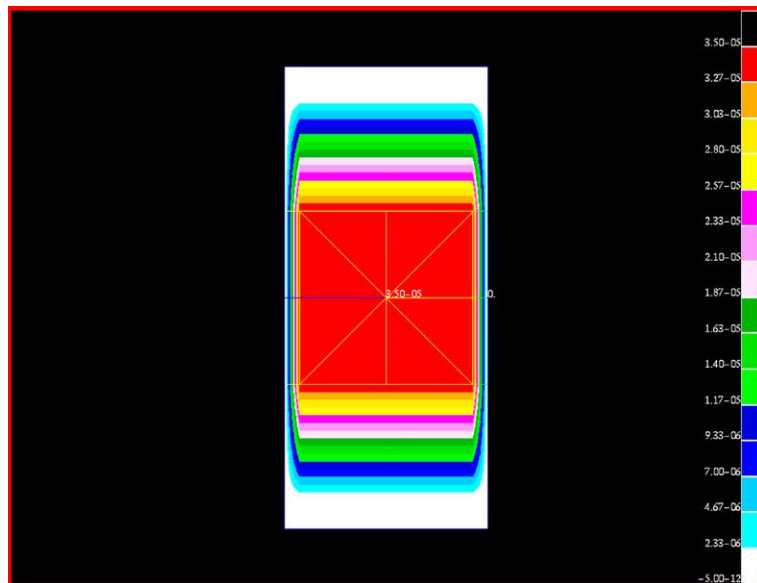


Fig. 5. Variation of V_1 component of Velocity Field I (Example 1).

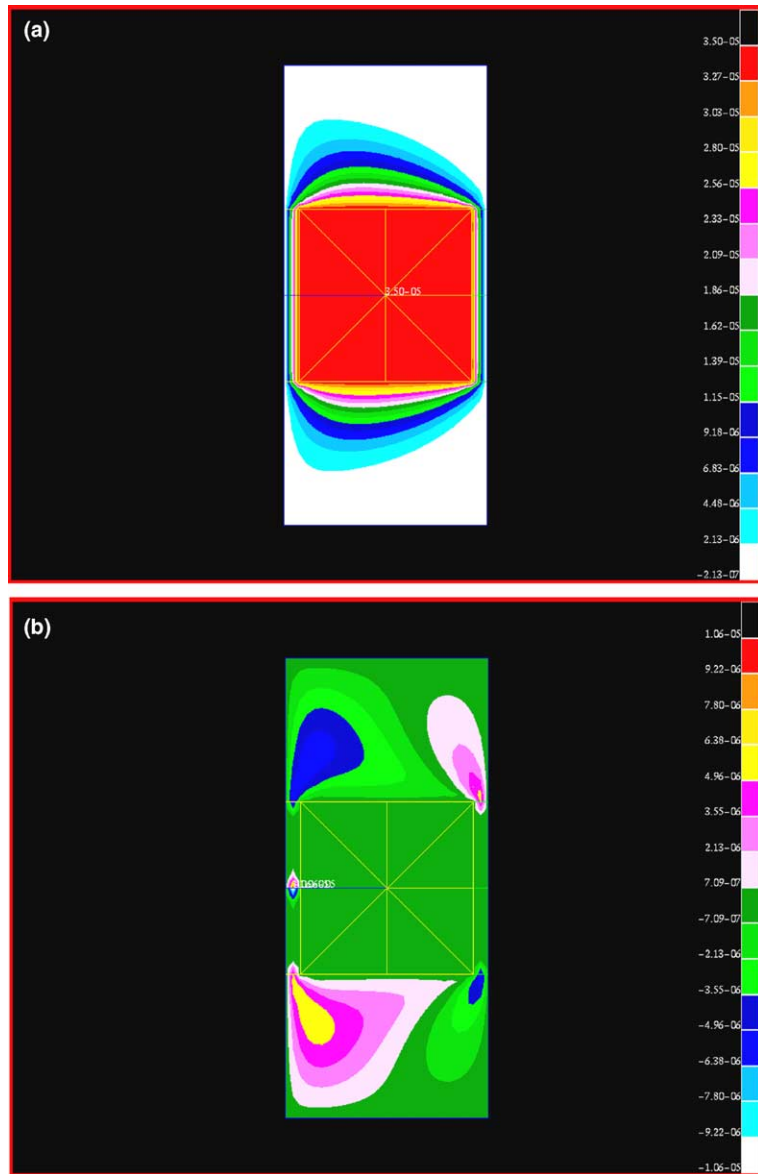


Fig. 6. Variation of Velocity Field II (Example 1); (a) V_1 component; (b) V_2 component.

5.2. Example 2: Slanted crack in a plate

Consider a slanted crack in a finite two-dimensional plate with length $L = 2$ units, width $W = 1$ unit and a 45-degree edge crack of normalized length $a/W = 0.4\sqrt{2}$, as shown in Fig. 7(a). The elastic modulus was assumed to follow an exponential function, given by

$$E(x_1) = \bar{E} \exp \left[\eta \left(x_1 - \frac{1}{2} \right) \right], \quad 0 \leq x_1 \leq W, \tag{66}$$

Table 1
Stress intensity factors and sensitivity of stress intensity factors for an edge-cracked plate (Velocity Field I, $b = 3.0$ units)

Method	E_2/E_1	SIF values		Sensitivity of SIF values			
		K_I	K_{II}	$\partial K_I/\partial a$		$\partial K_{II}/\partial a$	
		Present results	Present results	Proposed method	Finite difference	Proposed method	Finite difference
Method-I	0.01	69.8472	7.9892	16.3415	16.3417	1.0848	1.0848
	0.1	48.8555	6.1657	16.2291	16.2293	1.3624	1.3624
	0.2	43.8370	5.6612	15.9021	15.9023	1.4188	1.4188
	1.0	34.0637	4.5899	14.8104	14.8105	1.4995	1.4995
	5.0	26.3819	3.6370	13.4741	13.4743	1.5144	1.5144
	10.0	23.5686	3.2532	12.8719	12.8721	1.4992	1.4992
	100.0	15.8030	2.0810	10.8327	10.8329	1.3355	1.3355
Method-II	0.01	69.7959	8.0093	16.3247	16.3249	1.0865	1.0865
	0.1	48.8396	6.1716	16.2226	16.2228	1.3635	1.3635
	0.2	43.8277	5.6647	15.8980	15.8982	1.4196	1.4196
	1.0	34.0637	4.5899	14.8104	14.8105	1.4995	1.4995
	5.0	26.3850	3.6353	13.4754	13.4755	1.5135	1.5135
	10.0	23.5716	3.2510	12.8729	12.8730	1.4979	1.4979
	100.0	15.8016	2.0782	10.8288	10.8290	1.3320	1.3320

Table 2
Stress intensity factors and sensitivity of stress intensity factors for an edge-cracked plate (Velocity Field II, $b = 3.0$ units)

Method	E_2/E_1	SIF values		Sensitivity of SIF values			
		K_I	K_{II}	$\partial K_I/\partial a$		$\partial K_{II}/\partial a$	
		Present results	Present results	Proposed method	Finite difference	Proposed method	Finite difference
Method-I	0.01	69.8472	7.9892	16.3421	16.3423	1.0851	1.0851
	0.1	48.8555	6.1657	16.2291	16.2292	1.3625	1.3625
	0.2	43.8370	5.6612	15.9019	15.9021	1.4189	1.4189
	1.0	34.0637	4.5899	14.8101	14.8102	1.4996	1.4996
	5.0	26.3819	3.6370	13.4746	13.4747	1.5144	1.5144
	10.0	23.5686	3.2532	12.8731	12.8732	1.4992	1.4992
	100.0	15.8030	2.0810	10.8385	10.8386	1.3356	1.3356
Method-II	0.01	69.7959	8.0093	16.3254	16.3256	1.0866	1.0866
	0.1	48.8396	6.1716	16.2226	16.2228	1.3635	1.3635
	0.2	43.8277	5.6647	15.8979	15.8980	1.4196	1.4196
	1.0	34.0637	4.5899	14.8101	14.8102	1.4996	1.4996
	5.0	26.3850	3.6353	13.4759	13.4760	1.5136	1.5136
	10.0	23.5716	3.2510	12.8740	12.8742	1.4980	1.4980
	100.0	15.8016	2.0782	10.8348	10.8347	1.3323	1.3323

where \bar{E} and η are two material parameters. For numerical values, $\bar{E} = 1$ unit and $\eta = 0, 0.1, 0.25, 0.5, 0.75,$ and 1 were adopted. A plane stress condition was assumed. The applied load was prescribed along the upper edge with normal stress $\sigma_{22}(x_1, 1) = \bar{e}\bar{E} \exp[\eta(x_1 - 0.5)]$, where $\bar{e} = 1$. The displacement boundary condition was specified such that $u_2 = 0$ along the lower edge and, in addition, $u_1 = 0$ for the node at the right side of the lower edge.

Table 3
Stress intensity factors and sensitivity of stress intensity factors for an edge-cracked plate (Velocity Field I, $b = 2.33$ units)

Method	E_2/E_1	SIF values		Sensitivity of SIF values			
		K_I	K_{II}	$\partial K_I/\partial a$		$\partial K_{II}/\partial a$	
		Present results	Present results	Proposed method	Finite difference	Proposed method	Finite difference
Method-I	0.01	69.8435	7.9919	16.3386	16.3388	1.0843	1.0843
	0.1	48.8549	6.1659	16.2287	16.2289	1.3622	1.3622
	0.2	43.8370	5.6612	15.9020	15.9022	1.4187	1.4187
	1.0	34.0636	4.5898	14.8103	14.8105	1.4995	1.4995
	5.0	26.3806	3.6370	13.4730	13.4732	1.5143	1.5143
	10.0	23.5664	3.2531	12.8700	12.8701	1.4990	1.4990
	100.0	15.7970	2.0803	10.8264	10.8265	1.3341	1.3341
Method-II	0.01	69.7959	8.0093	16.3247	16.3249	1.0865	1.0865
	0.1	48.8396	6.1715	16.2225	16.2227	1.3634	1.3634
	0.2	43.8277	5.6647	15.8980	15.8982	1.4196	1.4196
	1.0	34.0636	4.5898	14.8103	14.8105	1.4995	1.4995
	5.0	26.3850	3.6352	13.4754	13.4755	1.5135	1.5135
	10.0	23.5716	3.2510	12.8728	12.8730	1.4978	1.4978
	100.0	15.8016	2.0782	10.8288	10.8290	1.3319	1.3320

Table 4
Stress intensity factors and sensitivity of stress intensity factors for an edge-cracked plate (Velocity Field I, $b = 1.74$ units)

Method	E_2/E_1	SIF values		Sensitivity of SIF values			
		K_I	K_{II}	$\partial K_I/\partial a$		$\partial K_{II}/\partial a$	
		Present results	Present results	Proposed method	Finite difference	Proposed method	Finite difference
Method-I	0.01	69.8419	7.9940	16.3374	16.3376	1.0844	1.0844
	0.1	48.8550	6.1662	16.2285	16.2287	1.3622	1.3622
	0.2	43.8372	5.6613	15.9020	15.9022	1.4186	1.4186
	1.0	34.0637	4.5898	14.8103	14.8105	1.4994	1.4994
	5.0	26.3798	3.6369	13.4724	13.4726	1.5142	1.5142
	10.0	23.5650	3.2530	12.8689	12.8691	1.4989	1.4989
	100.0	15.7937	2.0802	10.8232	10.8234	1.3336	1.3336
Method-II	0.01	69.7959	8.0092	16.3247	16.3249	1.0865	1.0865
	0.1	48.8396	6.1715	16.2225	16.2227	1.3634	1.3634
	0.2	43.8277	5.6646	15.8980	15.8982	1.4195	1.4195
	1.0	34.0637	4.5898	14.8103	14.8105	1.4994	1.4994
	5.0	26.3850	3.6352	13.4754	13.4755	1.5134	1.5134
	10.0	23.5716	3.2509	12.8728	12.8730	1.4978	1.4978
	100.0	15.8016	2.0781	10.8289	10.8290	1.3319	1.3319

Fig. 7(c) shows FEM discretization involving 1541 nodes, 460 8-noded quadrilateral elements, and 40 focused quarter-point 6-noded triangular elements. Methods I and II were both used to calculate the mixed-mode SIFs and their sensitivities with a domain size $2b \times 2b$ ($b = 0.2$ units), as shown in the Fig. 7(a). The velocity field (Velocity Field I) was computed by linear interpolation, defined as

Table 5
Stress intensity factors and sensitivity of stress intensity factors for an edge-cracked plate (Velocity Field I, $b = 1.22$ units)

Method	E_2/E_1	SIF values		Sensitivity of SIF values			
		K_I	K_{II}	$\partial K_I/\partial a$		$\partial K_{II}/\partial a$	
		Present results	Present results	Proposed method	Finite difference	Proposed method	Finite difference
Method-I	0.01	69.8429	7.9963	16.3371	16.3373	1.0845	1.0845
	0.1	48.8559	6.1667	16.2286	16.2288	1.3622	1.3622
	0.2	43.8380	5.6616	15.9022	15.9024	1.4186	1.4186
	1.0	34.0638	4.5897	14.8104	14.8106	1.4994	1.4994
	5.0	26.3791	3.6367	13.4721	13.4722	1.5142	1.5142
	10.0	23.5640	3.2528	12.8683	12.8685	1.4988	1.4988
	100.0	15.7914	2.0801	10.8215	10.8216	1.3335	1.3335
Method-II	0.01	69.7963	8.0092	16.3247	16.3250	1.0864	1.0864
	0.1	48.8399	6.1714	16.2226	16.2228	1.3634	1.3634
	0.2	43.8280	5.6645	15.8981	15.8983	1.4195	1.4195
	1.0	34.0638	4.5897	14.8104	14.8106	1.4994	1.4994
	5.0	26.3851	3.6351	13.4754	13.4756	1.5133	1.5133
	10.0	23.5717	3.2508	12.8729	12.8731	1.4977	1.4977
	100.0	15.8017	2.0780	10.8289	10.8291	1.3318	1.3318

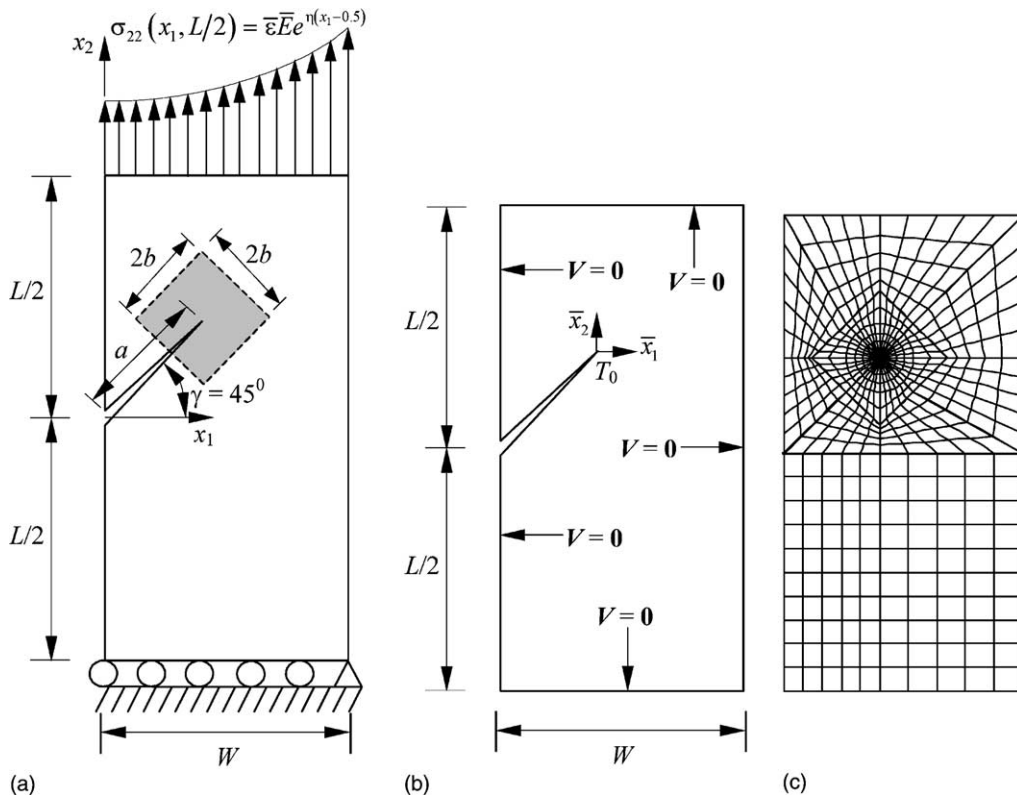


Fig. 7. Slanted crack in a plate; (a) geometry, loads, and domain size; (b) velocity field definition; and (c) FEM discretization (1785 nodes, 540 8-noded quadrilateral elements, and 40 focused quarter-point 6-noded triangular elements).

$$V_1(\bar{x}_1, \bar{x}_2) = \begin{cases} V_{1,\text{tip}} & \text{if } \bar{r} < 0.2829, \\ \frac{V_{1,\text{tip}}(0.4 - \bar{r})}{0.4 - 0.2829} & \text{if } 0.2829 > \bar{r} > 0.4, \\ 0 & \text{if } \bar{r} > 0.4 \end{cases} \quad (67)$$

and

$$V_2(\bar{x}_1, \bar{x}_2) = \begin{cases} V_{2,\text{tip}} & \text{if } \bar{r} < 0.2829, \\ \frac{V_{2,\text{tip}}(0.4 - \bar{r})}{0.4 - 0.2829} & \text{if } 0.2829 > \bar{r} > 0.4, \\ 0 & \text{if } \bar{r} > 0.4, \end{cases} \quad (68)$$

where the \bar{x}_1 – \bar{x}_2 axes are measured with respect to the crack tip T_0 , are oriented in the direction of the x_1 – x_2 axes, as shown in Fig. 7(b), and $\bar{r} = \sqrt{\bar{x}_1^2 + \bar{x}_2^2}$. In this example, a crack-tip velocity field $(V_{1,\text{tip}}, V_{2,\text{tip}}) = (10^{-5}a \cos \gamma, 10^{-5}a \sin \gamma)$ was used for sensitivity analysis. It can be seen from Eqs. (67) and (68) that the variation of the V_1 and V_2 components of the velocity field is similar over the entire domain of the plate. Fig. 8 schematically illustrates the variation of the V_1 component of the velocity field.

Table 6 provides a comparison of the predicted normalized SIFs $K_I/\bar{e}\bar{E}\sqrt{\pi a}$ and $K_{II}/\bar{e}\bar{E}\sqrt{\pi a}$ and the sensitivities of the SIFs, obtained by the proposed methods for several values of η . It is worth mentioning that the present results of normalized SIFs $K_I/\bar{e}\bar{E}\sqrt{\pi a}$ and $K_{II}/\bar{e}\bar{E}\sqrt{\pi a}$ are in good agreement with the reported results of Rao and Rahman [4], Eischen [29] and Kim and Paulino [30]. Table 6 contains two sets of results for $\partial K_I/\partial a$ and $\partial K_{II}/\partial a$. The first set of results is computed using the proposed methods (Method-I and Method-II) and the second is calculated using the finite-difference method. The results in Table 6 again demonstrate that continuum shape sensitivity analysis provides accurate estimates of $\partial K_I/\partial a$ and $\partial K_{II}/\partial a$, as compared with corresponding results from the finite-difference method for various values of η .

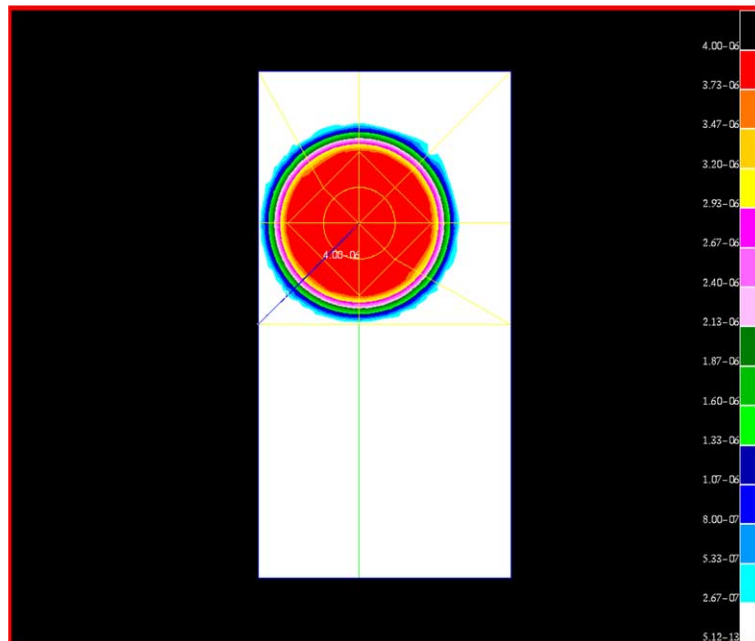


Fig. 8. Variation of V_1 component of Velocity Field (Example 2).

Table 6
Normalized stress intensity factors and sensitivity of stress intensity factors for a slanted crack in a plate

Method	η	Normalized SIF values		Sensitivity of SIF values			
		$\frac{K_I}{\sqrt{\pi a} \sqrt{\bar{E}}}$	$\frac{K_{II}}{\sqrt{\pi a} \sqrt{\bar{E}}}$	$\partial K_I / \partial a$		$\partial K_{II} / \partial a$	
		Present results	Present results	Proposed method	Finite difference	Proposed method	Finite difference
Method-I	0	1.4471	0.6145	6.1180	6.1180	1.7110	1.7110
	0.1	1.3915	0.5891	5.9268	5.9268	1.6559	1.6559
	0.25	1.3128	0.5533	5.6544	5.6544	1.5778	1.5778
	0.5	1.1931	0.4992	5.2359	5.2360	1.4594	1.4594
	0.75	1.0861	0.4513	4.8580	4.8580	1.3540	1.3540
	1	0.9904	0.4087	4.5162	4.5162	1.2601	1.2601
	10	0.1049	0.0415	1.0363	1.0363	0.3919	0.3919
Method-II	0	1.4471	0.6145	6.1180	6.1180	1.7110	1.7110
	0.1	1.3915	0.5892	5.9269	5.9268	1.6560	1.6560
	0.25	1.3128	0.5534	5.6544	5.6545	1.5782	1.5782
	0.5	1.1931	0.4994	5.2361	5.2361	1.4601	1.4601
	0.75	1.0861	0.4515	4.8581	4.8582	1.3550	1.3550
	1	0.9904	0.4090	4.5164	4.5164	1.2614	1.2614
	10	0.1049	0.0421	1.0366	1.0366	0.3978	0.3978

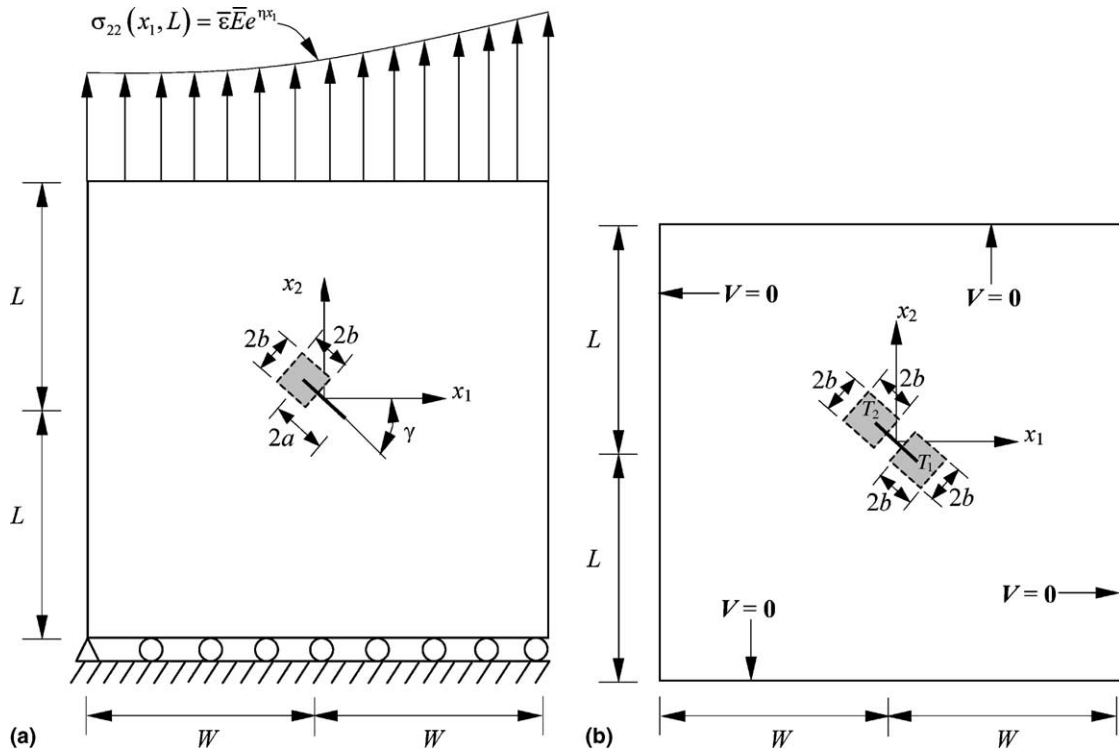


Fig. 9. Plate with an interior inclined crack; (a) geometry, loads, and domain size; and (b) velocity field definition.

5.3. Example 3: Plate with an interior inclined crack

Consider a centrally located inclined crack of length $2a = 2$ units and an orientation of γ in a finite two-dimensional square plate of size $2L = 2W = 20$ units, as shown in Fig. 9(a). A plane stress condition was assumed. The elastic modulus was assumed to be an exponential function, given by

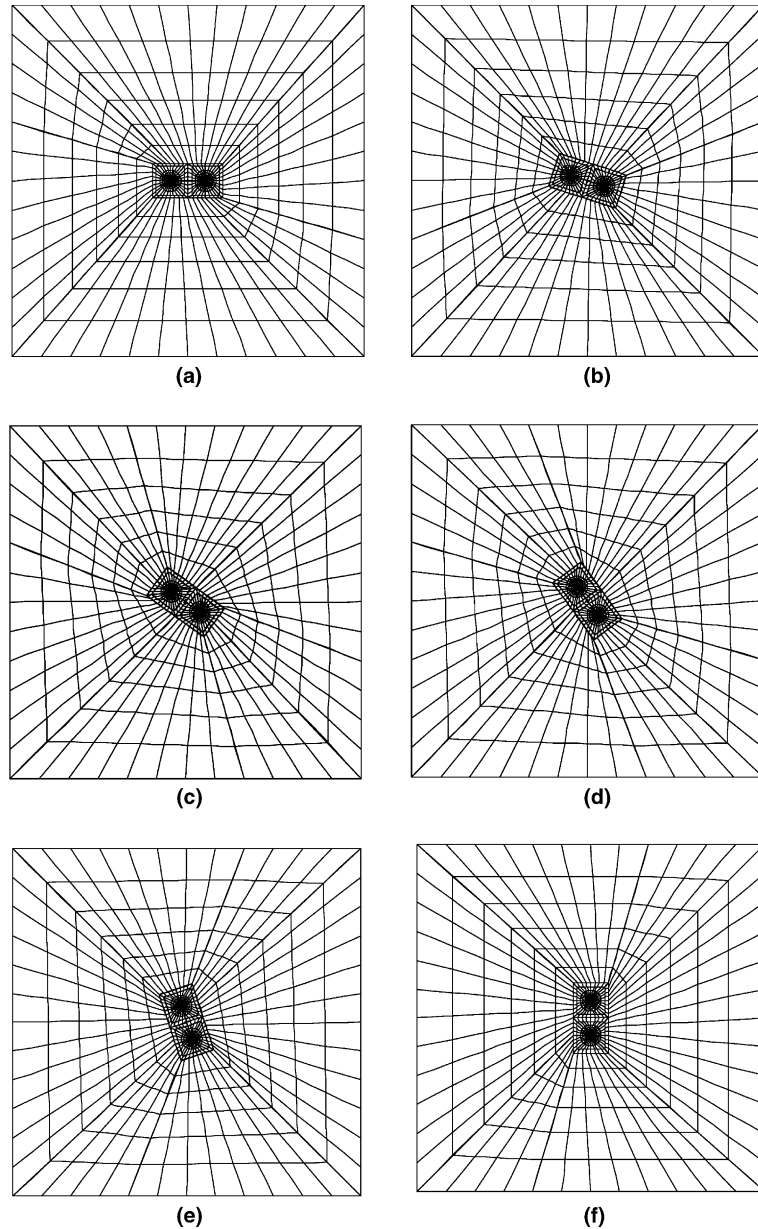


Fig. 10. FEM discretization for plate with an interior inclined crack; (a) $\gamma/\pi = 0$; (b) $\gamma/\pi = 0.1$; (c) $\gamma/\pi = 0.2$; (d) $\gamma/\pi = 0.3$; (e) $\gamma/\pi = 0.4$; and (f) $\gamma/\pi = 0.5$.

$$E(x_1) = \bar{E} \exp(\eta x_1), \quad -W \leq x_1 \leq W, \tag{69}$$

where \bar{E} and η are material parameters. The following data were used for the numerical study: $\bar{E} = 1$ unit; $\eta = 0.25$ and 0.5 ; and $\gamma/\pi = 0, 0.1, 0.2, 0.3, 0.4,$ and 0.5 . The applied load corresponds to $\sigma_{22}(x_1, 10) = \bar{\epsilon} \bar{E} \exp(\eta x_1)$, where $\bar{\epsilon} = 1$. This stress distribution was obtained by applying nodal forces along the top edge of the plate. The displacement boundary condition was prescribed such that $u_2 = 0$ along the lower edge and, in addition, $u_1 = 0$ for the node at the left hand side of the lower edge. This loading results in a uniform strain $\epsilon_{22}(x_1, x_2) = \bar{\epsilon}$ in a corresponding uncracked structure.

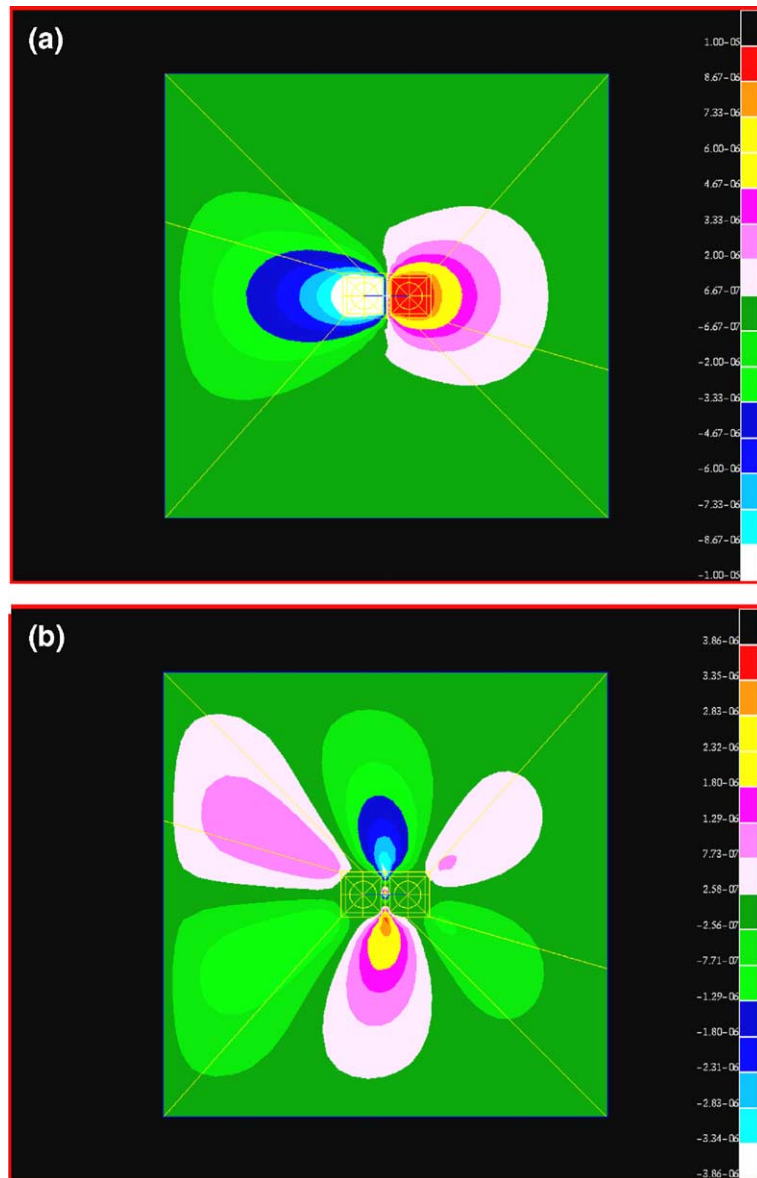


Fig. 11. Variation of Velocity Field (Example 3); (a) V_1 component; (b) V_2 component.

The velocity field was obtained from an FEM analysis. The FEM analysis was performed by prescribing a velocity field (V_{1tip}, V_{2tip}), evaluated at the right crack-tip, at all points in the domain $2b \times b$ surrounding the right crack tip, and a velocity field ($-V_{1tip}, -V_{2tip}$), at all points in the domain $2b \times b$ surrounding the left crack-tip, as shown in Fig. 9(b). A zero velocity field was prescribed at all points on the boundary. A velocity field ($V_{1,tip}, V_{2,tip}$) = ($10^{-5}a \cos \gamma, -10^{-5}a \sin \gamma$) was used for the sensitivity analysis. The same FEM discretization used in the regular analysis was adopted to obtain the velocity field.

Fig. 10(a)–(f) shows the FEM discretization involving 2416 nodes, 736 8-noded quadrilateral elements, and 64 focused quarter-point 6-noded triangular elements, adopted for $\gamma/\pi = 0, 0.1, 0.2, 0.3, 0.4$ and 0.5 , respectively. Both Methods I and II were used to calculate the mixed-mode SIFs and their sensitivities with a domain size $2b \times 2b$ ($b = 1.0$ units), as shown in Fig. 9(a). Fig. 11(a) and (b) shows the contour plot of the variation of the V_1 and V_2 components of velocity field over the entire domain of the interior inclined cracked plate with $\gamma/\pi = 0$, when a velocity field (V_{1tip}, V_{2tip}) is prescribed at the right crack-tip.

Table 7

Normalized stress intensity factors and sensitivity of stress intensity factors for a inclined interior crack in a plate ($\eta = 0.25$, Method-I)

Method	γ/π	Normalized SIF values			
		$\frac{K_I(+a)}{\bar{E} \bar{\epsilon} \sqrt{\pi a}}$	$\frac{K_I(-a)}{\bar{E} \bar{\epsilon} \sqrt{\pi a}}$	$\frac{K_{II}(+a)}{\bar{E} \bar{\epsilon} \sqrt{\pi a}}$	$\frac{K_{II}(-a)}{\bar{E} \bar{\epsilon} \sqrt{\pi a}}$
Present results Method-I [$M^{(1,2)}$]	0	1.2207	0.8396	-0.0003	-0.0002
	0.1	1.1015	0.7622	-0.3275	-0.2577
	0.2	0.7919	0.5565	-0.5223	-0.4255
	0.3	0.4174	0.2946	-0.5103	-0.4396
	0.4	0.1207	0.0768	-0.3052	-0.2829
	0.5	0.0008	0.0008	0.0003	-0.0003
Konda and Erdogan [31]	0	1.196	0.825	0	0
	0.1	1.081	0.750	-0.321	-0.254
	0.2	0.781	0.548	-0.514	-0.422
	0.3	0.414	0.290	-0.504	-0.437
	0.4	0.121	0.075	-0.304	-0.282
	0.5	0	0	0	0
Proposed Method-I [$\dot{M}^{(1,2)}$]	Sensitivity of SIF values				
		$\frac{\partial K_I(+a)}{\partial a}$	$\frac{\partial K_I(-a)}{\partial a}$	$\frac{\partial K_{II}(+a)}{\partial a}$	$\frac{\partial K_{II}(-a)}{\partial a}$
	0	1.5549	0.5018	0.0030	-0.0033
	0.1	1.3970	0.4599	-0.3485	-0.1739
	0.2	0.9900	0.3471	-0.5483	-0.2992
	0.3	0.5126	0.1870	-0.5184	-0.3304
	0.4	0.1513	0.0407	-0.2981	-0.2288
	0.5	-0.0007	-0.0008	-0.0007	0.0007
	0	1.5549	0.5018	0.0030	-0.0033
	0.1	1.3970	0.4599	-0.3485	-0.1739
	0.2	0.9900	0.3471	-0.5483	-0.2992
	0.3	0.5126	0.1870	-0.5184	-0.3304
	0.4	0.1513	0.0407	-0.2981	-0.2288
	0.5	-0.0007	-0.0008	-0.0007	0.0007

Table 8

Normalized stress intensity factors and sensitivity of stress intensity factors for a inclined interior crack in a plate ($\eta = 0.25$, Method-II)

Method	γ/π	Normalized SIF values			
		$\frac{K_I(+a)}{\bar{E}\bar{\epsilon}\sqrt{\pi a}}$	$\frac{K_I(-a)}{\bar{E}\bar{\epsilon}\sqrt{\pi a}}$	$\frac{K_{II}(+a)}{\bar{E}\bar{\epsilon}\sqrt{\pi a}}$	$\frac{K_{II}(-a)}{\bar{E}\bar{\epsilon}\sqrt{\pi a}}$
Present results Method-II [$M^{(1,2)}$]	0	1.2208	0.8395	-0.0003	-0.0002
	0.1	1.1015	0.7621	-0.3277	-0.2575
	0.2	0.7919	0.5565	-0.5226	-0.4253
	0.3	0.4174	0.2947	-0.5105	-0.4395
	0.4	0.1206	0.0769	-0.3053	-0.2828
	0.5	0.0008	0.0008	0.0003	-0.0003
Konda and Erdogan [31]	0	1.196	0.825	0	0
	0.1	1.081	0.750	-0.321	-0.254
	0.2	0.781	0.548	-0.514	-0.422
	0.3	0.414	0.290	-0.504	-0.437
	0.4	0.121	0.075	-0.304	-0.282
	0.5	0	0	0	0
Sensitivity of SIF values					
		$\frac{\partial K_I(+a)}{\partial a}$	$\frac{\partial K_I(-a)}{\partial a}$	$\frac{\partial K_{II}(+a)}{\partial a}$	$\frac{\partial K_{II}(-a)}{\partial a}$
Proposed Method-II [$M^{(1,2)}$]	0	1.5552	0.5016	0.0030	-0.0033
	0.1	1.3972	0.4597	-0.3484	-0.1740
	0.2	0.9901	0.3471	-0.5482	-0.2993
	0.3	0.5126	0.1870	-0.5184	-0.3304
	0.4	0.1513	0.0408	-0.2982	-0.2287
	0.5	-0.0007	-0.0008	-0.0009	0.0009
Finite difference	0	1.5552	0.5016	0.0030	-0.0033
	0.1	1.3972	0.4597	-0.3484	-0.1740
	0.2	0.9901	0.3471	-0.5482	-0.2993
	0.3	0.5126	0.1870	-0.5184	-0.3304
	0.4	0.1513	0.0408	-0.2982	-0.2287
	0.5	-0.0007	-0.0008	-0.0009	0.0009

Konda and Erdogan [31] investigated an infinite plate with such a configuration for SIFs. Obviously, an FEM model cannot represent the infinite domains addressed in their analysis, but as long as the ratios a/W and a/L are kept relatively small (e.g. $a/W = a/L \leq 1/10$), the approximation is acceptable. Tables 7 and 8 provide a comparison between predicted normalized SIFs $K_I(a)/\bar{E}\bar{\epsilon}\sqrt{\pi a}$ and $K_I(-a)/\bar{E}\bar{\epsilon}\sqrt{\pi a}$ for both crack tips obtained by Methods I and II, respectively, and those of Konda and Erdogan [31] for several values of γ/π , when $\eta = 0.25$. Tables 7 and 8 also provide a comparison between the predicted sensitivities of SIFs obtained by the proposed methods for both crack tips for several values of γ/π , when $\eta = 0.25$. Table 7 contains two sets of results for $\partial K_I/\partial a$ and $\partial K_{II}/\partial a$. The first set is computed using the proposed methods (Method-I and Method-II), while the second set is calculated using the finite-difference method. Tables 9 and 10 present similar results for normalized SIFs $K_I(a)/\bar{E}\bar{\epsilon}\sqrt{\pi a}$ and $K_I(-a)/\bar{E}\bar{\epsilon}\sqrt{\pi a}$ and the sensitivities of SIFs for various values of γ/π , when $\eta = 0.5$. The results in Tables 7–10 demonstrate that continuum shape sensitivity analysis provides accurate estimates of $\partial K_I/\partial a$ and $\partial K_{II}/\partial a$ when compared with corresponding results from the finite-difference method for various values of crack lengths and material inhomogeneity parameters.

Table 9

Normalized stress intensity factors and sensitivity of stress intensity factors for a inclined interior crack in a plate ($\eta = 0.5$, Method-I)

Method	γ/π	Normalized SIF values			
		$\frac{K_I(+a)}{\bar{E} \bar{\epsilon} \sqrt{\pi a}}$	$\frac{K_I(-a)}{\bar{E} \bar{\epsilon} \sqrt{\pi a}}$	$\frac{K_{II}(+a)}{\bar{E} \bar{\epsilon} \sqrt{\pi a}}$	$\frac{K_{II}(-a)}{\bar{E} \bar{\epsilon} \sqrt{\pi a}}$
Present results Method-I [$M^{(1,2)}$]	0	1.4463	0.6797	-0.0036	0.0019
	0.1	1.3009	0.6234	-0.3524	-0.2128
	0.2	0.9303	0.4650	-0.5556	-0.3655
	0.3	0.4893	0.2498	-0.5352	-0.3971
	0.4	0.1446	0.0608	-0.3122	-0.2694
	0.5	0.0009	0.0009	0.0008	-0.0007
Konda and Erdogan [31]	0	1.424	0.674	0	0
	0.1	1.285	0.617	-0.344	-0.213
	0.2	0.925	0.460	-0.548	-0.365
	0.3	0.490	0.247	-0.532	-0.397
	0.4	0.146	0.059	-0.314	-0.269
	0.5	0	0	0	0
Sensitivity of SIF values					
		$\frac{\partial K_I(+a)}{\partial a}$	$\frac{\partial K_I(-a)}{\partial a}$	$\frac{\partial K_{II}(+a)}{\partial a}$	$\frac{\partial K_{II}(-a)}{\partial a}$
Proposed Method-I [$M^{(1,2)}$]	0	2.2609	0.1238	-0.0058	0.0025
	0.1	2.0148	0.1351	-0.4096	-0.0614
	0.2	1.4080	0.1384	-0.6295	-0.1477
	0.3	0.7197	0.0905	-0.5815	-0.2194
	0.4	0.2142	0.0080	-0.3216	-0.1888
	0.5	-0.0019	-0.0021	-0.0011	0.0011
Finite difference	0	2.2609	0.1238	-0.0058	0.0025
	0.1	2.0148	0.1351	-0.4096	-0.0614
	0.2	1.4080	0.1384	-0.6295	-0.1477
	0.3	0.7197	0.0905	-0.5815	-0.2194
	0.4	0.2142	0.0080	-0.3216	-0.1887
	0.5	-0.0019	-0.0021	-0.0011	0.0011

6. Summary and conclusions

Two new methods are presented for predicting the first-order sensitivity of Mode-I and Mode-II stress-intensity factors for a crack in isotropic, linear-elastic functionally graded materials. These methods involve the material derivative concept from continuum mechanics, domain integral representation of interaction integrals, known as the M -integral, and direct differentiation. Unlike virtual crack extension techniques, no mesh perturbation is needed in the proposed methods to calculate the sensitivity of stress-intensity factors. Since the governing variational equation is differentiated prior to discretization, the resulting sensitivity equations are independent of such approximate numerical techniques as the meshless method, the finite element method, the boundary element method, or others. Three examples are presented to calculate the first-order derivative of stress-intensity factors. Results show that first-order sensitivities of stress intensity factors obtained using the proposed method are in excellent agreement with the reference solutions obtained from finite-difference methods for the structural and crack geometries considered in this study.

Table 10

Normalized stress intensity factors and sensitivity of stress intensity factors for a inclined interior crack in a plate ($\eta = 0.5$, Method-II)

Method	γ/π	Normalized SIF values			
		$\frac{K_I(+a)}{E \bar{v} \sqrt{\pi a}}$	$\frac{K_I(-a)}{E \bar{v} \sqrt{\pi a}}$	$\frac{K_{II}(+a)}{E \bar{v} \sqrt{\pi a}}$	$\frac{K_{II}(-a)}{E \bar{v} \sqrt{\pi a}}$
Present results Method-II [$M^{(1,2)}$]	0	1.4465	0.6796	-0.0036	0.0019
	0.1	1.3010	0.6234	-0.3529	-0.2125
	0.2	0.9303	0.4650	-0.5562	-0.3651
	0.3	0.4892	0.2499	-0.5356	-0.3969
	0.4	0.1445	0.0608	-0.3124	-0.2693
	0.5	0.0009	0.0009	0.0008	-0.0007
Konda and Erdogan [31]	0	1.424	0.674	0	0
	0.1	1.285	0.617	-0.344	-0.213
	0.2	0.925	0.460	-0.548	-0.365
	0.3	0.490	0.247	-0.532	-0.397
	0.4	0.146	0.059	-0.314	-0.269
	0.5	0	0	0	0
Sensitivity of SIF values					
		$\frac{\partial K_I(+a)}{\partial a}$	$\frac{\partial K_I(-a)}{\partial a}$	$\frac{\partial K_{II}(+a)}{\partial a}$	$\frac{\partial K_{II}(-a)}{\partial a}$
Proposed Method-II [$M^{(1,2)}$]	0	2.2616	0.1236	-0.0058	0.0025
	0.1	2.0154	0.1349	-0.4094	-0.0615
	0.2	1.4083	0.1383	-0.6293	-0.1478
	0.3	0.7196	0.0905	-0.5816	-0.2194
	0.4	0.2141	0.0080	-0.3219	-0.1886
	0.5	-0.0019	-0.0021	-0.0015	0.0015
Finite difference	0	2.2616	0.1235	-0.0058	0.0025
	0.1	2.0154	0.1349	-0.4094	-0.0615
	0.2	1.4083	0.1383	-0.6293	-0.1478
	0.3	0.7196	0.0905	-0.5816	-0.2194
	0.4	0.2141	0.0080	-0.3219	-0.1886
	0.5	-0.0019	-0.0021	-0.0015	0.0015

Acknowledgment

The authors would like to acknowledge the financial support of the US National Science Foundation (NSF) under Award Nos. CMS-9733058 and CMS-04094632.

Appendix A

The p -functions

$$p_1 = \sigma_{11}^{(1)} \frac{\partial z_1^{(2)}}{\partial x_1} \frac{\partial q}{\partial x_1}, \quad p_2 = \sigma_{12}^{(1)} \frac{\partial z_1^{(2)}}{\partial x_1} \frac{\partial q}{\partial x_2}, \quad p_3 = \sigma_{21}^{(1)} \frac{\partial z_1^{(2)}}{\partial x_1} \frac{\partial q}{\partial x_1}, \quad p_4 = \sigma_{22}^{(1)} \frac{\partial z_1^{(2)}}{\partial x_1} \frac{\partial q}{\partial x_2},$$

$$\begin{aligned}
p_5 &= \sigma_{11}^{(2)} \frac{\partial z_1^{(1)}}{\partial x_1} \frac{\partial q}{\partial x_1}, & p_6 &= \sigma_{12}^{(2)} \frac{\partial z_1^{(1)}}{\partial x_1} \frac{\partial q}{\partial x_2}, & p_7 &= \sigma_{21}^{(2)} \frac{\partial z_2^{(1)}}{\partial x_1} \frac{\partial q}{\partial x_1}, & p_8 &= \sigma_{22}^{(2)} \frac{\partial z_2^{(1)}}{\partial x_1} \frac{\partial q}{\partial x_2}, \\
p_9 &= -\frac{1}{2} \sigma_{11}^{(2)} \varepsilon_{11}^{(1)} \frac{\partial q}{\partial x_1}, & p_{10} &= -\sigma_{12}^{(2)} \varepsilon_{12}^{(1)} \frac{\partial q}{\partial x_1}, & p_{11} &= -\frac{1}{2} \sigma_{22}^{(2)} \varepsilon_{22}^{(1)} \frac{\partial q}{\partial x_1}, & p_{12} &= -\frac{1}{2} \sigma_{11}^{(1)} \varepsilon_{11}^{(2)} \frac{\partial q}{\partial x_1}, \\
p_{13} &= -\sigma_{12}^{(1)} \varepsilon_{12}^{(2)} \frac{\partial q}{\partial x_1}, & p_{14} &= -\frac{1}{2} \sigma_{22}^{(1)} \varepsilon_{22}^{(2)} \frac{\partial q}{\partial x_1}, & p_{15} &= \sigma_{11}^{(1)} \frac{\partial \varepsilon_{11}^{(2)}}{\partial x_1} q, & p_{16} &= 2\sigma_{12}^{(1)} \frac{\partial \varepsilon_{12}^{(2)}}{\partial x_1}, \\
p_{17} &= \sigma_{22}^{(1)} \frac{\partial \varepsilon_{22}^{(2)}}{\partial x_1} q, & p_{18} &= -\frac{\partial \sigma_{11}^{(2)}}{\partial x_1} \varepsilon_{11}^{(1)} q, & p_{19} &= -2 \frac{\partial \sigma_{12}^{(2)}}{\partial x_1} \varepsilon_{12}^{(1)} q, & p_{20} &= -\frac{\partial \sigma_{22}^{(2)}}{\partial x_1} \varepsilon_{22}^{(1)} q, \\
p_{21} &= \sigma_{11}^{(2)} \frac{\partial \varepsilon_{11}^{(1)}}{\partial x_1} q, & p_{22} &= 2\sigma_{12}^{(2)} \frac{\partial \varepsilon_{12}^{(1)}}{\partial x_1}, & p_{23} &= \sigma_{22}^{(2)} \frac{\partial \varepsilon_{22}^{(1)}}{\partial x_1} q, & p_{24} &= -\frac{\partial \sigma_{11}^{(1)}}{\partial x_1} \varepsilon_{11}^{(2)} q, \\
p_{25} &= -2 \frac{\partial \sigma_{12}^{(1)}}{\partial x_1} \varepsilon_{12}^{(2)} q, & p_{26} &= -\frac{\partial \sigma_{22}^{(1)}}{\partial x_1} \varepsilon_{22}^{(2)} q.
\end{aligned} \tag{A.1}$$

The P -functions

$$P_1 = \dot{\sigma}_{11}^{(1)} \frac{\partial z_1^{(2)}}{\partial x_1} \frac{\partial q}{\partial x_1} + \sigma_{11}^{(1)} \frac{\partial \dot{z}_1^{(2)}}{\partial x_1} \frac{\partial q}{\partial x_1}, \tag{A.2}$$

$$P_2 = \dot{\sigma}_{12}^{(1)} \frac{\partial z_1^{(2)}}{\partial x_1} \frac{\partial q}{\partial x_2} + \sigma_{12}^{(1)} \frac{\partial \dot{z}_1^{(2)}}{\partial x_1} \frac{\partial q}{\partial x_2}, \tag{A.3}$$

$$P_3 = \dot{\sigma}_{21}^{(1)} \frac{\partial z_2^{(2)}}{\partial x_1} \frac{\partial q}{\partial x_1} + \sigma_{21}^{(1)} \frac{\partial \dot{z}_2^{(2)}}{\partial x_1} \frac{\partial q}{\partial x_1}, \tag{A.4}$$

$$P_4 = \dot{\sigma}_{22}^{(1)} \frac{\partial z_2^{(2)}}{\partial x_1} \frac{\partial q}{\partial x_2} + \sigma_{22}^{(1)} \frac{\partial \dot{z}_2^{(2)}}{\partial x_1} \frac{\partial q}{\partial x_2}, \tag{A.5}$$

$$P_5 = \sigma_{11}^{(2)} \frac{\partial \dot{z}_1}{\partial x_1} \frac{\partial q}{\partial x_1}, \tag{A.6}$$

$$P_6 = \sigma_{12}^{(2)} \frac{\partial \dot{z}_1}{\partial x_1} \frac{\partial q}{\partial x_2}, \tag{A.7}$$

$$P_7 = \sigma_{12}^{(2)} \frac{\partial \dot{z}_2^{(1)}}{\partial x_1} \frac{\partial q}{\partial x_1}, \tag{A.8}$$

$$P_8 = \sigma_{22}^{(2)} \frac{\partial \dot{z}_2^{(1)}}{\partial x_1} \frac{\partial q}{\partial x_2}, \tag{A.9}$$

$$P_9 = -\frac{1}{2} \sigma_{11}^{(2)} \dot{\varepsilon}_{11}^{(1)} \frac{\partial q}{\partial x_1}, \tag{A.10}$$

$$P_{10} = -\sigma_{12}^{(2)} \dot{\varepsilon}_{12}^{(1)} \frac{\partial q}{\partial x_1}, \tag{A.11}$$

$$P_{11} = -\frac{1}{2} \sigma_{22}^{(2);(1)} \dot{\varepsilon}_{22} \frac{\partial q}{\partial x_1}, \quad (\text{A.12})$$

$$P_{12} = -\frac{1}{2} \dot{\sigma}_{11}^{(1)} \varepsilon_{11}^{(2)} \frac{\partial q}{\partial x_1} - \frac{1}{2} \sigma_{11}^{(1)} \dot{\varepsilon}_{11}^{(2)} \frac{\partial q}{\partial x_1}, \quad (\text{A.13})$$

$$P_{13} = -\dot{\sigma}_{12}^{(1)} \varepsilon_{12}^{(2)} \frac{\partial q}{\partial x_1} - \sigma_{12}^{(1)} \dot{\varepsilon}_{12}^{(2)} \frac{\partial q}{\partial x_1}, \quad (\text{A.14})$$

$$P_{14} = -\frac{1}{2} \dot{\sigma}_{22}^{(1)} \varepsilon_{22}^{(2)} \frac{\partial q}{\partial x_1} - \frac{1}{2} \sigma_{22}^{(1)} \dot{\varepsilon}_{22}^{(2)} \frac{\partial q}{\partial x_1}, \quad (\text{A.15})$$

$$P_{15} = \dot{\sigma}_{11}^{(1)} \frac{\partial \varepsilon_{11}^{(2)}}{\partial x_1} q + \sigma_{11}^{(1)} \frac{\partial \dot{\varepsilon}_{11}^{(2)}}{\partial x_1} q, \quad (\text{A.16})$$

$$P_{16} = 2\dot{\sigma}_{12}^{(1)} \frac{\partial \varepsilon_{12}^{(2)}}{\partial x_1} q + \sigma_{12}^{(1)} \frac{\partial \dot{\varepsilon}_{12}^{(2)}}{\partial x_1} q, \quad (\text{A.17})$$

$$P_{17} = \dot{\sigma}_{22}^{(1)} \frac{\partial \varepsilon_{22}^{(2)}}{\partial x_1} q + \sigma_{22}^{(1)} \frac{\partial \dot{\varepsilon}_{22}^{(2)}}{\partial x_1} q, \quad (\text{A.18})$$

$$P_{18} = -\frac{\partial \sigma_{11}^{(2)}}{\partial x_1} \dot{\varepsilon}_{11}^{(1)} q, \quad (\text{A.19})$$

$$P_{19} = -2 \frac{\partial \sigma_{12}^{(2)}}{\partial x_1} \dot{\varepsilon}_{12}^{(1)} q, \quad (\text{A.20})$$

$$P_{20} = -\frac{\partial \sigma_{22}^{(2)}}{\partial x_1} \dot{\varepsilon}_{22}^{(1)} q, \quad (\text{A.21})$$

$$P_{21} = \sigma_{11}^{(2)} \frac{\partial \dot{\varepsilon}_{11}^{(1)}}{\partial x_1} q, \quad (\text{A.22})$$

$$P_{22} = 2\sigma_{12}^{(2)} \frac{\partial \dot{\varepsilon}_{12}^{(1)}}{\partial x_1} q, \quad (\text{A.23})$$

$$P_{23} = \sigma_{22}^{(2)} \frac{\partial \dot{\varepsilon}_{22}^{(1)}}{\partial x_1} q, \quad (\text{A.24})$$

$$P_{24} = -\frac{\partial \dot{\sigma}_{11}^{(1)}}{\partial x_1} \varepsilon_{11}^{(2)} q - \frac{\partial \sigma_{11}^{(1)}}{\partial x_1} \dot{\varepsilon}_{11}^{(2)} q, \quad (\text{A.25})$$

$$P_{25} = -2 \frac{\partial \dot{\sigma}_{12}^{(1)}}{\partial x_1} \varepsilon_{12}^{(2)} q - 2 \frac{\partial \sigma_{12}^{(1)}}{\partial x_1} \dot{\varepsilon}_{12}^{(2)} q, \quad (\text{A.26})$$

$$P_{26} = -\frac{\partial \dot{\sigma}_{22}^{(1)}}{\partial x_1} \varepsilon_{22}^{(2)} q - \frac{\partial \sigma_{22}^{(1)}}{\partial x_1} \dot{\varepsilon}_{22}^{(2)} q, \quad (\text{A.27})$$

where

$$\varepsilon_{11}^{(1)} = \frac{\partial z_1^{(1)}}{\partial x_1}, \quad (\text{A.28})$$

$$\varepsilon_{12}^{(1)} = \frac{1}{2} \left(\frac{\partial z_2^{(1)}}{\partial x_1} + \frac{\partial z_1^{(1)}}{\partial x_2} \right), \quad (\text{A.29})$$

$$\varepsilon_{22}^{(1)} = \frac{\partial z_2^{(1)}}{\partial x_2}, \quad (\text{A.30})$$

$$\frac{\partial \varepsilon_{11}^{(1)}}{\partial x_1} = \frac{\partial^2 z_1^{(1)}}{\partial x_1^2}, \quad (\text{A.31})$$

$$\frac{\partial \varepsilon_{12}^{(1)}}{\partial x_1} = \frac{1}{2} \left(\frac{\partial^2 z_2^{(1)}}{\partial x_1^2} + \frac{\partial^2 z_1^{(1)}}{\partial x_1 \partial x_2} \right), \quad (\text{A.32})$$

$$\frac{\partial \varepsilon_{22}^{(1)}}{\partial x_1} = \frac{\partial^2 z_2^{(1)}}{\partial x_1 \partial x_2}, \quad (\text{A.33})$$

$$\dot{\varepsilon}_{11}^{(1)} = \frac{\partial \dot{z}_1^{(1)}}{\partial x_1}, \quad (\text{A.34})$$

$$\dot{\varepsilon}_{12}^{(1)} = \frac{1}{2} \left(\frac{\partial \dot{z}_1^{(1)}}{\partial x_2} + \frac{\partial \dot{z}_2^{(1)}}{\partial x_1} \right), \quad (\text{A.35})$$

$$\dot{\varepsilon}_{22}^{(1)} = \frac{\partial \dot{z}_2^{(1)}}{\partial x_2}, \quad (\text{A.36})$$

$$\frac{\partial \dot{\varepsilon}_{11}^{(1)}}{\partial x_1} = \frac{\partial^2 \dot{z}_1^{(1)}}{\partial x_1^2}, \quad (\text{A.37})$$

$$\frac{\partial \dot{\varepsilon}_{12}^{(1)}}{\partial x_1} = \frac{1}{2} \left(\frac{\partial^2 \dot{z}_2^{(1)}}{\partial x_1^2} + \frac{\partial^2 \dot{z}_1^{(1)}}{\partial x_1 \partial x_2} \right), \quad (\text{A.38})$$

$$\frac{\partial \dot{\varepsilon}_{22}^{(1)}}{\partial x_1} = \frac{\partial^2 \dot{z}_2^{(1)}}{\partial x_1 \partial x_2}, \quad (\text{A.39})$$

$$\sigma_{ij}^{(1)} = D_{ijkl}(\mathbf{x}) \varepsilon_{kl}^{(1)}, \quad (\text{A.40})$$

$$\dot{\sigma}_{ij}^{(1)} = \dot{D}_{ijkl}(\mathbf{x}) \varepsilon_{kl}^{(1)} + D_{ijkl}(\mathbf{x}) \dot{\varepsilon}_{kl}^{(1)}, \quad (\text{A.41})$$

$$\frac{\partial \sigma_{ij}^{(1)}}{\partial x_1} = \frac{\partial D_{ijkl}}{\partial x_1}(\mathbf{x}) \varepsilon_{kl}^{(1)} + D_{ijkl}(\mathbf{x}) \frac{\partial \varepsilon_{kl}^{(1)}}{\partial x_1}, \quad (\text{A.42})$$

$$\frac{\partial \dot{\sigma}_{ij}^{(1)}}{\partial x_1} = \frac{\partial \dot{D}_{ijkl}(\mathbf{x})}{\partial x_1} \varepsilon_{kl}^{(1)} + \frac{\partial D_{ijkl}(\mathbf{x})}{\partial x_1} \dot{\varepsilon}_{kl}^{(1)} + \dot{D}_{ijkl}(\mathbf{x}) \frac{\partial \varepsilon_{kl}^{(1)}}{\partial x_1} + D_{ijkl}(\mathbf{x}) \frac{\partial \dot{\varepsilon}_{kl}^{(1)}}{\partial x_1}, \quad (\text{A.43})$$

$$D_{ijkl}(\mathbf{x}) = \begin{cases} \frac{E(\mathbf{x})}{1-\nu^2} \begin{bmatrix} 1 & \nu & 0 \\ \nu & 1 & 0 \\ 0 & 0 & \frac{1-\nu}{2} \end{bmatrix} & \text{for plane stress,} \\ \frac{E(\mathbf{x})}{(1+\nu)(1-2\nu)} \begin{bmatrix} 1-\nu & \nu & 0 \\ \nu & 1-\nu & 0 \\ 0 & 0 & \frac{1-2\nu}{2} \end{bmatrix} & \text{for plane strain,} \end{cases} \quad (\text{A.44})$$

$$\dot{D}_{ijkl}(\mathbf{x}) = \frac{\dot{E}(\mathbf{x})}{E(\mathbf{x})} D_{ijkl}(\mathbf{x}), \quad (\text{A.45})$$

$$\frac{\partial \dot{D}_{ijkl}(\mathbf{x})}{\partial x_1} = \frac{\dot{E}_{,1}(\mathbf{x})}{E(\mathbf{x})} D_{ijkl}(\mathbf{x}), \quad (\text{A.46})$$

$$\dot{E}_{,1}(\mathbf{x}) = \frac{\partial}{\partial x_1} \left(\frac{\partial E(\mathbf{x})}{\partial x_1} \right) V_1 + \frac{\partial}{\partial x_2} \left(\frac{\partial E(\mathbf{x})}{\partial x_1} \right) V_2, \quad (\text{A.47})$$

$$\varepsilon_{11}^{(2)} = \frac{\partial z_1^{(2)}}{\partial x_1}, \quad (\text{A.48})$$

$$\varepsilon_{12}^{(2)} = \frac{1}{2} \left(\frac{\partial z_2^{(2)}}{\partial x_1} + \frac{\partial z_1^{(2)}}{\partial x_2} \right), \quad (\text{A.49})$$

$$\varepsilon_{22}^{(2)} = \frac{\partial z_2^{(2)}}{\partial x_2}, \quad (\text{A.50})$$

$$\frac{\partial \varepsilon_{11}^{(2)}}{\partial x_1} = \frac{\partial^2 z_1^{(2)}}{\partial x_1^2}, \quad (\text{A.51})$$

$$\frac{\partial \varepsilon_{12}^{(2)}}{\partial x_1} = \frac{1}{2} \left(\frac{\partial^2 z_2^{(2)}}{\partial x_1^2} + \frac{\partial^2 z_1^{(2)}}{\partial x_1 \partial x_2} \right), \quad (\text{A.52})$$

$$\frac{\partial \varepsilon_{22}^{(2)}}{\partial x_1} = \frac{\partial^2 z_2^{(2)}}{\partial x_1 \partial x_2}, \quad (\text{A.53})$$

$$\dot{\varepsilon}_{ij}^{(2)} = -\frac{\dot{E}_{\text{tip}}}{E_{\text{tip}}} \varepsilon_{ij}^{(2)} \quad (\text{A.54})$$

and

$$\frac{\partial \dot{\varepsilon}_{ij}^{(2)}}{\partial x_1} = -\frac{\dot{E}_{\text{tip}}}{E_{\text{tip}}} \frac{\partial \varepsilon_{ij}^{(2)}}{\partial x_1}, \quad (\text{A.55})$$

with \dot{E}_{tip} being equal to \dot{E} evaluated at the crack tip. In equations p_{1-26} and P_{1-26} , $E = E(x_1)$ and $\nu = \text{constant}$. When $E = \text{constant}$, p_{15-26} and P_{15-26} vanish, as expected. Hence p_{1-24} and P_{1-14} degenerate to corresponding equations for homogeneous materials [22].

Appendix B

The s -functions

$$\begin{aligned}
 s_1 &= \sigma_{11}^{(1)} \frac{\partial z_1^{(2)}}{\partial x_1} \frac{\partial q}{\partial x_1}, & s_2 &= \sigma_{12}^{(1)} \frac{\partial z_1^{(2)}}{\partial x_1} \frac{\partial q}{\partial x_2}, & s_3 &= \sigma_{21}^{(1)} \frac{\partial z_2^{(2)}}{\partial x_1} \frac{\partial q}{\partial x_1}, \\
 s_4 &= \sigma_{22}^{(1)} \frac{\partial z_2^{(2)}}{\partial x_1} \frac{\partial q}{\partial x_2}, & s_5 &= \sigma_{12}^{(2)} \frac{\partial z_1^{(1)}}{\partial x_1} \frac{\partial q}{\partial x_2}, & s_6 &= \sigma_{22}^{(2)} \frac{\partial z_2^{(1)}}{\partial x_1} \frac{\partial q}{\partial x_2}, \\
 s_7 &= \sigma_{12}^{(2)} \frac{\partial z_1^{(1)}}{\partial x_2} \frac{\partial q}{\partial x_1}, & s_8 &= \sigma_{22}^{(2)} \frac{\partial z_2^{(1)}}{\partial x_2} \frac{\partial q}{\partial x_1}, & s_9 &= \sigma_{11}^{(1)} \left(\frac{\partial \varepsilon_{11}^{(2)}}{\partial x_1} - \frac{\partial \tilde{\varepsilon}_{11}^{(2)}}{\partial x_1} \right) q, \\
 s_{10} &= 2\sigma_{12}^{(1)} \left(\frac{\partial \varepsilon_{12}^{(2)}}{\partial x_1} - \frac{\partial \tilde{\varepsilon}_{12}^{(2)}}{\partial x_1} \right) q, & s_{11} &= \sigma_{22}^{(1)} \left(\frac{\partial \varepsilon_{22}^{(2)}}{\partial x_1} - \frac{\partial \tilde{\varepsilon}_{22}^{(2)}}{\partial x_1} \right) q, & s_{12} &= \frac{1}{E} \frac{\partial E}{\partial x_1} \sigma_{11}^{(2)} \varepsilon_{11}^{(1)} q, \\
 s_{13} &= \frac{2}{E} \frac{\partial E}{\partial x_1} \sigma_{12}^{(2)} \varepsilon_{12}^{(1)} q, & s_{14} &= \frac{1}{E} \frac{\partial E}{\partial x_1} \sigma_{22}^{(2)} \varepsilon_{22}^{(1)} q.
 \end{aligned} \tag{B.1}$$

The S -functions

$$S_1 = \dot{\sigma}_{11}^{(1)} \frac{\partial z_1^{(2)}}{\partial x_1} \frac{\partial q}{\partial x_1} + \sigma_{11}^{(1)} \frac{\partial \dot{z}_1^{(2)}}{\partial x_1} \frac{\partial q}{\partial x_1}, \tag{B.2}$$

$$S_2 = \dot{\sigma}_{12}^{(1)} \frac{\partial z_1^{(2)}}{\partial x_1} \frac{\partial q}{\partial x_2} + \sigma_{12}^{(1)} \frac{\partial \dot{z}_1^{(2)}}{\partial x_1} \frac{\partial q}{\partial x_2}, \tag{B.3}$$

$$S_3 = \dot{\sigma}_{21}^{(1)} \frac{\partial z_2^{(2)}}{\partial x_1} \frac{\partial q}{\partial x_1} + \sigma_{21}^{(1)} \frac{\partial \dot{z}_2^{(2)}}{\partial x_1} \frac{\partial q}{\partial x_1}, \tag{B.4}$$

$$S_4 = \dot{\sigma}_{22}^{(1)} \frac{\partial z_2^{(2)}}{\partial x_1} \frac{\partial q}{\partial x_2} + \sigma_{22}^{(1)} \frac{\partial \dot{z}_2^{(2)}}{\partial x_1} \frac{\partial q}{\partial x_2}, \tag{B.5}$$

$$S_5 = \sigma_{12}^{(2)} \frac{\partial \dot{z}_1}{\partial x_1} \frac{\partial q}{\partial x_2}, \tag{B.6}$$

$$S_6 = \sigma_{22}^{(2)} \frac{\partial \dot{z}_2^{(1)}}{\partial x_1} \frac{\partial q}{\partial x_2}, \tag{B.7}$$

$$S_7 = -\sigma_{12}^{(2)} \frac{\partial \dot{z}_1^{(1)}}{\partial x_2} \frac{\partial q}{\partial x_1}, \tag{B.8}$$

$$S_8 = -\sigma_{22}^{(2)} \frac{\partial \dot{z}_2^{(1)}}{\partial x_2} \frac{\partial q}{\partial x_1}, \tag{B.9}$$

$$S_9 = \dot{\sigma}_{11}^{(1)} \left(\frac{\partial \varepsilon_{11}^{(2)}}{\partial x_1} - \frac{\partial \tilde{\varepsilon}_{11}^{(2)}}{\partial x_1} \right) q + \sigma_{11}^{(1)} \left(\frac{\partial \dot{\varepsilon}_{11}^{(2)}}{\partial x_1} - \frac{\partial \dot{\tilde{\varepsilon}}_{11}^{(2)}}{\partial x_1} \right) q, \quad (\text{B.10})$$

$$S_{10} = 2\dot{\sigma}_{12}^{(1)} \left(\frac{\partial \varepsilon_{12}^{(2)}}{\partial x_1} - \frac{\partial \tilde{\varepsilon}_{12}^{(2)}}{\partial x_1} \right) q + 2\sigma_{12}^{(1)} \left(\frac{\partial \dot{\varepsilon}_{12}^{(2)}}{\partial x_1} - \frac{\partial \dot{\tilde{\varepsilon}}_{12}^{(2)}}{\partial x_1} \right) q, \quad (\text{B.11})$$

$$S_{11} = \dot{\sigma}_{22}^{(1)} \left(\frac{\partial \varepsilon_{22}^{(2)}}{\partial x_1} - \frac{\partial \tilde{\varepsilon}_{22}^{(2)}}{\partial x_1} \right) q + \sigma_{22}^{(1)} \left(\frac{\partial \dot{\varepsilon}_{22}^{(2)}}{\partial x_1} - \frac{\partial \dot{\tilde{\varepsilon}}_{22}^{(2)}}{\partial x_1} \right) q, \quad (\text{B.12})$$

$$S_{12} = \frac{1}{E} \frac{\partial E}{\partial x_1} \sigma_{11}^{(2)} \dot{\varepsilon}_{11}^{(1)} q, \quad (\text{B.13})$$

$$S_{13} = 2 \frac{1}{E} \frac{\partial E}{\partial x_1} \sigma_{12}^{(2)} \dot{\varepsilon}_{12}^{(1)} q, \quad (\text{B.14})$$

$$S_{14} = \frac{1}{E} \frac{\partial E}{\partial x_1} \sigma_{22}^{(2)} \dot{\varepsilon}_{22}^{(1)} q, \quad (\text{B.15})$$

where $\varepsilon_{ij}^{(1)}$, $\dot{\varepsilon}_{ij}^{(1)}$, $\partial \varepsilon_{ij}^{(1)} / \partial x_1$, $\partial \dot{\varepsilon}_{ij}^{(1)} / \partial x_1$, $\sigma_{ij}^{(1)}$, $\dot{\sigma}_{ij}^{(1)}$, $\partial \sigma_{ij}^{(1)} / \partial x_1$, $\partial \dot{\sigma}_{ij}^{(1)} / \partial x_1$, $\varepsilon_{ij}^{(2)}$, $\dot{\varepsilon}_{ij}^{(2)}$, $\partial \varepsilon_{ij}^{(2)} / \partial x_1$, $\partial \dot{\varepsilon}_{ij}^{(2)} / \partial x_1$ can be computed as described in [Appendix A](#),

$$\frac{\partial \tilde{\varepsilon}_{ij}^{(2)}}{\partial x_1} = \frac{\partial C_{ijkl}(\mathbf{x})}{\partial x_1} \sigma_{kl}^{(2)} + C_{ijkl}(\mathbf{x}) \frac{\partial \sigma_{kl}^{(2)}}{\partial x_1} \quad (\text{B.16})$$

and

$$\frac{\partial \dot{\tilde{\varepsilon}}_{ij}^{(2)}}{\partial x_1} = - \frac{\dot{E}(\mathbf{x})}{E(\mathbf{x})} \frac{\partial \tilde{\varepsilon}_{ij}^{(2)}}{\partial x_1}. \quad (\text{B.17})$$

In equations s_1 – s_{14} and S_1 – S_{14} , $E = E(x_1)$ and $\nu = \text{constant}$. When $E = \text{constant}$, s_9 – s_{14} and S_9 – S_{14} vanish, as expected. Hence s_1 – s_8 and S_1 – S_8 degenerate to corresponding equations for homogeneous materials [22].

References

- [1] S. Suresh, A. Mortensen, *Fundamentals of Functionally Graded Materials*, IOM Communications Ltd., London, 1998.
- [2] F. Erdogan, Fracture mechanics of functionally graded materials, *Comp. Engrg.* 5 (7) (1995) 753–770.
- [3] G.H. Paulino, Fracture of functionally graded materials, *Engrg. Fract. Mech.* 69 (14–16) (2002) 1519–1520.
- [4] B.N. Rao, S. Rahman, Meshfree analysis of cracks in isotropic functionally graded materials, *Engrg. Fract. Mech.* 70 (2003) 1–27.
- [5] B.N. Rao, S. Rahman, An interaction integral method for analysis of cracks in orthotropic functionally graded materials, *Comput. Mech.* 32 (2003) 40–51.
- [6] H.O. Madsen, S. Krenk, N.C. Lind, *Methods of Structural Safety*, Prentice-Hall, Englewood Cliffs, New Jersey, 1986.
- [7] M. Grigoriu, M.T.A. Saif, S. El-Borgi, A. Ingrassia, Mixed-mode fracture initiation and trajectory prediction under random stresses, *Int. J. Fract.* 45 (1990) 19–34.
- [8] J.W. Provan, *Probabilistic Fracture Mechanics and Reliability*, Martinus Nijhoff Publishers, Dordrecht, The Netherlands, 1987.
- [9] G.H. Besterfield, W.K. Liu, M.A. Lawrence, T. Belytschko, Fatigue crack growth reliability by probabilistic finite elements, *Comput. Methods Appl. Mech. Engrg.* 86 (1991) 297–320.
- [10] G.H. Besterfield, M.A. Lawrence, T. Belytschko, Brittle fracture reliability by probabilistic finite elements, *ASCE J. Engrg. Mech.* 116 (3) (1990) 642–659.

- [11] S. Rahman, A stochastic model for elastic–plastic fracture analysis of circumferential through-wall-cracked pipes subject to bending, *Engrg. Fract. Mech.* 52 (2) (1995) 265–288.
- [12] S. Rahman, J.-S. Kim, Probabilistic fracture mechanics for nonlinear structures, *Int. J. Pressure Vessels Piping* 78 (4) (2000) 9–17.
- [13] S. Rahman, Probabilistic fracture mechanics by J -estimation and finite element methods, *Engrg. Fract. Mech.* 68 (2001) 107–125.
- [14] S.C. Lin, J. Abel, Variational approach for a new direct-integration form of the virtual crack extension method, *Int. J. Fract.* 38 (1988) 217–235.
- [15] H.G. deLorenzi, On the energy release rate and the J -integral for 3-D crack configurations, *Int. J. Fract.* 19 (1982) 183–193.
- [16] H.G. deLorenzi, Energy release rate calculations by the finite element method, *Engrg. Fract. Mech.* 21 (1985) 129–143.
- [17] R.B. Haber, H.M. Koh, Explicit expressions for energy release rates using virtual crack extensions, *Int. J. Numer. Methods Engrg.* 21 (1985) 301–315.
- [18] E.J. Barbero, J.N. Reddy, The Jacobian derivative method for three-dimensional fracture mechanics, *Commun. Appl. Numer. Methods* 6 (1990) 507–518.
- [19] C.G. Hwang, P.A. Wawrzynek, A.K. Tayebi, A.R. Ingraffea, On the virtual crack extension method for calculation of the rates of energy release rate, *Engrg. Fract. Mech.* 59 (1998) 521–542.
- [20] G. Chen, S. Rahman, Y.H. Park, Shape sensitivity analysis of linear-elastic cracked structures, *ASME J. Pressure Vessel Technol.* 124 (4) (2002) 476–482.
- [21] G. Chen, S. Rahman, Y.H. Park, Shape sensitivity and reliability analyses of linear-elastic cracked structures, *Int. J. Fract.* 112 (3) (2001) 223–246.
- [22] G. Chen, S. Rahman, Y.H. Park, Shape sensitivity analysis in mixed-mode fracture mechanics, *Comput. Mech.* 27 (4) (2001) 282–291.
- [23] B.N. Rao, S. Rahman, Continuum shape sensitivity analysis of mode-I fracture in functionally graded materials, in: *Proceedings of 2003 ASME Pressure Vessels and Piping Conference*, Cleveland, OH, July 20–24, 2003.
- [24] K.K. Choi, E.J. Haug, Shape design sensitivity analysis of elastic structures, *J. Struct. Mech.* 11 (2) (1983) 231–269.
- [25] E.J. Haug, K.K. Choi, V. Komkov, *Design Sensitivity Analysis of Structural Systems*, Academic Press, New York, NY, 1986.
- [26] J.H. Hou, J.S. Sheen, On the design velocity field in the domain and boundary methods for shape optimization, *AIAA J.* (88-2338) (1988) 1032–1040.
- [27] K.K. Choi, K.H. Chang, A study of design velocity field computation for shape optimal design, *Finite Elements Anal. Des.* 15 (1994) 317–341.
- [28] J.J. Rodenas, F.J. Fuenmayor, J.E. Tarancon, A numerical methodology to assess the quality of the design velocity field computation methods in shape sensitivity analysis, *Int. J. Numer. Methods Engrg.* 59 (2004) 1725–1747.
- [29] J.W. Eischen, Fracture of nonhomogeneous materials, *Int. J. Fract.* 34 (1987) 3–22.
- [30] J.H. Kim, G.H. Paulino, Finite element evaluation of mixed mode stress intensity factors in functionally graded materials, *Int. J. Numer. Methods Engrg.* 53 (8) (2002) 1903–1935.
- [31] N. Konda, F. Erdogan, The mixed mode crack problem in a nonhomogeneous elastic medium, *Engrg. Fract. Mech.* 47 (4) (1994) 533–545.